Physics – Uspekhi **60** (11) 1121 – 1146 (2017)

REVIEWS OF TOPICAL PROBLEMS PACS numbers: 71.20.Be, **71.70. – d**, **75.10. – b**

Orbital physics in transition metal compounds: new trends

S V Streltsov, D I Khomskii

DOI: https://doi.org/10.3367/UFNe.2017.08.038196

Contents

1. Introduction **1121**

2. Basic concepts in the description of electrons in solids **1122**

3. Basic effects related to the orbital degrees of freedom **1124**

3.1 Crystal-field splitting, spin-state transitions; 3.2 Orbital degrees of freedom and magnetism; 3.3 Double exchange; 3.4 Jahn–Teller effect; 3.5 Spin–orbit coupling

4. Effective reduction of dimensionality due to orbital degrees of freedom and its consequences **1131**

4.1 Formation of low-dimensional magnetic systems due to orbital ordering; 4.2 '1D-zation' of electron spectrum and orbitally driven Peierls state; 4.3 Novel states close to the Mott transition: 'molecules' in solids

5. Orbital-selective effects **1136**

5.1 Orbital-selective Mott transition; 5.2 Orbital-selective behavior and (partial) suppression of magnetism

6. Spin–orbit-related effects **1141**

6.1 Spin–orbit coupling versus Jahn–Teller effect; 6.2 Spin–orbit coupling and the formation of 'molecules' in solids; 6.3 $J_{\text{eff}} = 1/2$ and the spin–orbit-assisted Mott state; 6.4 Spin–orbit-driven Peierls transition; 6.5 Kitaev exchange; 6.6 Singlet (or excitonic) magnetism

7. Conclusions **1144**

References **1145**

Abstract. The present review discusses different effects related to orbital degrees of freedom. Leaving aside such aspects as the superexchange mechanism of cooperative Jahn–Teller distortions and various properties of 'Kugel–Khomskii'-like models, we mostly concentrate on other phenomena, which are the focus of modern condensed matter physics. After a general introduction, we start with a discussion of the concept of effective reduction of dimensionality due to orbital degrees of freedom and consider such phenomena as the orbitally driven Peierls effect and the formation of small clusters of ions in the vicinity of the Mott transition, which behave like 'molecules' embedded in a solid. The second large part is devoted to orbital-selective effects, such as the orbital-selective Mott transition and the suppression of magnetism due to the fact that the electrons on some orbitals start to form singlet molecular orbitals. At the end, the rapidly growing field of so-called 'spin–orbit-dominated' transition metal compounds is briefly reviewed, including such topics as the interplay between the spin–orbit coupling and the Jahn–Teller effect, the formation of the spin–orbit-driven Mott and Peierls states, the role of orbital degrees of freedom in generating the Kitaev exchange coupling, and the singlet (excitonic) magnetism in 4d and 5d transition metal compounds.

Keywords: orbital ordering, spin-orbit coupling, transition-metal oxides

S V Streltsov Mikheev Institute of Metal Physics,
Ural Branch of the Russian Academy of Sciences,
ul. S Kovalevskoi 18, 620108 Ekaterinburg, Russian Federation;
Ural Federal University, named after
the First President of Russia B N Yeltsin,
ul. Mira 19, 620002 Ekaterinburg, Russian Federation
D I Khomskii University of Cologne, Institute of Physics II,
Zülpicher Str. 77, D-50937, Cologne, Germany
E-mail: streltsov@imp.uran.ru, khomskii@ph2.uni-koeln.de

Received 17 July 2017, revised 1 August 2017
Uspekhi Fizicheskikh Nauk **187** (11) 1205 – 1235 (2017)
DOI: https://doi.org/10.3367/UFNr.2017.08.038196
Translated by S V Streltsov; edited by A Radzig

1. Introduction

Systems with strongly correlated electrons, in particular, transition metal (TM) compounds, present a very interesting class of materials with extremely rich properties (see, e.g., Refs [1, 2]). Among them are metals, insulators (of a special kind), and systems with metal–insulator transitions; they exhibit different types of ordering [magnetic, charge ordering (CO), orbital ordering (OO)], the cooperative Jahn–Teller effect, and, last but not least, high-temperature superconductivity. All this richness is mainly due to strong electron correlations and the presence in them, and mutual interplay, of different degrees of freedom: charge, spin, and orbital, and all of this, of course, on the background of the lattice, with which all these electronic degrees of freedom often strongly interact.

The crucial general feature of these systems is the fundamental importance of electron–electron interaction, which determines the main properties of these systems, changes the behavior of electrons compared with that following from the standard free-electron-like or band description, and leads to localization of electrons on respective sites. These are the famous Mott, or Mott–Hubbard, insulators. Most often, such electron localization leads to the appearance of localized magnetic moments,

which then determine all the rich magnetic properties of Mott insulators, and sometimes gives also rise to charge ordering. The existence of two different limiting cases – strongly correlated and localized electrons, as opposed to weakly interacting itinerant ones — also leads to the possibility of a phase transition between these states, caused by a change in temperature, pressure, doping, etc.: the famous Mott metal–insulator transition (MIT).

Besides charge and spin degrees of freedom, in real TM compounds one also has to take into account orbital degrees of freedom, which lead to many nontrivial consequences — orbital ordering, a directional character of many properties, nontrivial effects related to the relativistic spin–orbit coupling (SOC). All these effects taken together can lead to novel, very interesting phenomena, which are the subject of the present review. For example, the directional character of orbitals may result in a spontaneous reduction of dimensionality, when three-dimensional $KCuF_3$ or $Tl_2Ru_2O_7$ start to behave like one-dimensional magnets. This effect, together with another very interesting phenomenon — the formation of small clusters, where electrons are practically delocalized, while a system as a whole is still insulating — are discussed in Section 4. This concept of 'molecules in solids,' leading to a 'stepwise' Mott transition, is an alternative to a homogeneous Mott transition.

Another important aspect of Mott physics is discussed in Section 5. This is the so-called orbital-selective Mott transition, when due to the directional character of the orbitals there is a substantial overlap between some of orbitals centered on different sites, while hopping (and, hence, the bandwidth) between the others is much smaller, so that they turn out to be more susceptible to the Mott transition, which again occurs stepwise, but in a momentum space, first for narrow and then for wider bands. Moreover, even if there is no Mott transition, this separation into more and less 'localized' orbitals (in fact, it is the electrons, not the orbitals, which can be localized or itinerant) may strongly affect the magnetic properties of a system, resulting, in particular, in a suppression of the double exchange mechanism of ferromagnetism.

Finally, there is a large group of effects related to spin–orbit coupling (see Section 6), which is under intensive study right now and which has already brought up such phenomena as the spin–orbit-assisted Mott state and Kitaev and excitonic magnetism.

The present review is devoted to a general description of the main concepts of 'orbital physics', with the main focus being new developments in this rather large area of condensed matter physics. We describe novel phenomena mentioned above and also discuss many real examples of systems, the properties of which find a natural explanation using these concepts. For completeness, to make our review more self-contained, we also included in the first two introductory sections a general description of the main concepts in the field of systems with strongly correlated electrons, in particular, TM compounds, paying the main attention to the role of orbital degrees of freedom in different phenomena. A more complete presentation of this material can be found in many monographs and textbooks, in particular, in Refs [1, 3–5], and in review articles [6–9]. We do not discuss here in detail possible types and mechanisms of orbital ordering and the extensive literature devoted to 'Kugel–Khomskii' and compass models. The first topic is reviewed in rather old but not yet obsolete paper [7] and in recent book [1]. For other aspects of orbital physics, we may recommend reviews [10, 11].

2. Basic concepts in the description of electrons in solids

To start with, we discuss at the beginning general ways to describe the state of electrons in solids in different situations. The simplest approach, from which a description of electrons is always started, is that of free electrons (band structure theory). In this type of treatment, one considers the motion of an electron in a periodic lattice potential, first ignoring electron–electron interaction or treating it in a mean-field way. This leads to a well-known formation of energy bands — the regions of allowed states, in general divided by the forbidden regions, energy gaps.

There are two main approaches for describing these energy bands: the weak coupling approximation, in which a periodic potential of the lattice is treated as a perturbation, and the tight-binding approximation. For our purposes, in particular, for describing d-electrons of TM compounds, the second method is more appropriate, and we will mostly use it below. When we start with the band description, we can easily get both insulating and metallic states by filling available band states. According to the Pauli principle we can put two electrons with spins 'up' and 'down' in each state. If some bands turn out to be partially filled, we are dealing with a metal, like Na or Al. And if some bands are completely filled, and the upper-lying bands separated from the occupied ones by an energy gap are empty, we have a band insulator or semiconductor like Ge or Si.

In the tight-binding approximation, we can speak of bands which are formed by intersite hopping of electrons between particular ionic states, e.g., 1s states of hydrogen or 3d states of TM ions. For lattice of N sites, each such (nondegenerate) band would contain N electronic states, into each of which we can put two electrons, so that there are places for $2N$ electrons in such a band, e.g., a 1s band of a lattice made of equally separated hydrogen ions (protons) (Fig. 1a). Corresponding tightly bound electrons can be described by the Hamiltonian

$$H = -t \sum_{\langle ij \rangle \sigma} c^{\dagger}_{i\sigma} c_{j\sigma} \,, \tag{1}$$

where $c^{\dagger}_{i\sigma}$ and $c_{j\sigma}$ are the creation and annihilation electron operators on sites i and j. The intersite hopping matrix element t is positive for s orbitals. Summation in the formula (1) goes over all inequivalent pairs of nearest-neighbor lattice sites, numerated by indexes i and j. In momentum space, the Hamiltonian takes the form

$$H = \sum_{\mathbf{k}\sigma} \varepsilon(\mathbf{k})\, c^{\dagger}_{\mathbf{k}\sigma} c_{\mathbf{k}\sigma} \tag{2}$$

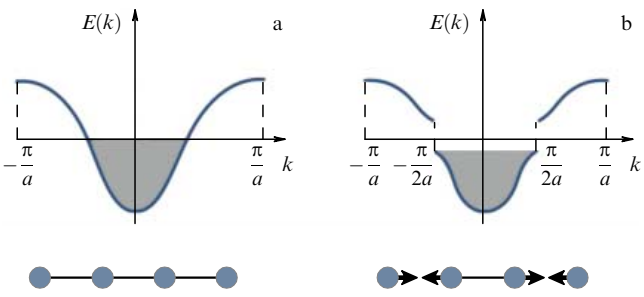

Figure 1. Peierls transition accompanied by an opening of the gap in the electronic spectrum $E(k)$. Distance between sites in the uniform chain is a.

with the dispersion $\varepsilon(\mathbf{k}) = -2t\cos(k_x a)$. If we have a noninteger or odd number of electrons per site, e.g., one electron as for a lattice of hydrogen ions, the band will necessarily be partially (e.g., half-) filled, and we will have a metal. Only if we have an even number of electrons per site will such a system be a usual band insulator (but even in this case in a realistic situation it is possible to obtain a metal or semimetal, if some bands overlap).

In this band picture, one can also have metal–insulator transitions; these may be caused by structural transitions with lattice distortions, which opens a gap exactly at the Fermi surface. The simplest example is the Peierls transition in a one-dimensional (1D) case. If we have, for example, a regular chain of sites (e.g., hydrogen atoms) with, say, one electron per site, then the 1s band would be half-filled (Fig. 1a). Dimerization of this chain (a first step towards the formation of H_2 molecules from the chain of hydrogen atoms) would open the gap exactly at the Fermi surface and would decrease electron energy (Fig. 1b), and this decrease overcomes the loss of lattice (deformation) energy, i.e., such a chain would always be unstable to the dimerization (see also review [12]). We note right away that such an instability in a chain would develop not only for a half-filled band, but also for other fillings: e.g., for the band filled by 1/3 or 2/3, we would have trimerization, and for the 1/4-filled band – tetramerization. We will see real examples of such phenomena later on, in Section 4.2.

Such metal–insulator transitions in the band picture may occur not only for 1D- or (quasi)-1D systems, but also in a more general situation. The usual condition for their appearance is the so-called nesting of the Fermi surface, which means that some parts of the Fermi surface coincide when shifted by a certain vector $\mathbf{Q}$. In this case, a superstructure with this wave vector $\mathbf{Q}$ could be formed — a charge density wave (CDW) in the case of effective electron attraction (e.g., via phonons) or a spin density wave (SDW) for electron repulsion. And if the gap which opens at these transitions cut the whole Fermi surface, it would lead to a metal–insulator transition. Such examples are encountered in some TM dichalcogenides, such as TaS_2.

Therefore, according to the band picture, if there is no dimerization, the regular lattice of hydrogen atoms with one electron per site should have half-filled band and should be metallic, irrespective of the distance between atoms or of the value of the intersite hopping matrix element t, which for large distances between sites would be exponentially small. Of course, this contradicts common sense: we should instead deal here with a collection of individual (hydrogen) atoms with electrons localized one per lattice site.

The reason for this was explained already long ago [13] (see also Appendix A.1 in book [1]): when we remember that electrons repel each other, it immediately becomes clear that, if we start with one electron per site and then try to create charge carriers, transferring an electron from this site to the other one, the repulsion of the transferred electron with 'its own' one, already existing at this site, will prevent such a charge transfer. In effect, the material would become an insulator with each electron localized at its own site. This is what we now call Mott or Mott–Hubbard insulators. And, in contrast to the band insulators described at the beginning of this section, the very fact that such a system remains insulating is due to electron–electron interactions, and not due to the interaction of independent electrons with the periodic lattice potential.

To treat this state, we have to generalize the description given by Eqns (1), (2) and include electron–election interactions — at least the Coulomb repulsion between electrons at the same site. The corresponding model

$$H = -t\sum_{\langle ij\rangle\,\sigma} c^{\dagger}_{i\sigma}c_{j\sigma} + U\sum_{i} n_{i\uparrow}n_{i\downarrow}\,, \tag{3}$$

where $n_{i\sigma} = c^{\dagger}_{i\sigma}c_{i\sigma}$ is the electron density, is called the Hubbard model, and it serves nowadays as the basic model to describe the physics of systems with strong electron–electron interactions or with strong electron correlations.

According to the physics discussed above and described by the Hubbard model (3), the state of the system is characterized by two parameters: the average electron density $n = N_{\rm el}/N$, and the effective interaction U/t, or U/W, where $W = 2zt$ is the electron bandwidths (for simple lattices like linear chain, square, or cubic lattices; and z is the number of nearest neighbors). Here, N is the number of sites, and $N_{\rm el}$ is the number of electrons. If $U/t \ll 1$, we are dealing with weakly interacting electrons, and in this case the standard band description is valid; electron–electron interaction can then be taken into account by the perturbation theory, using, for example, the Feynman diagram technique, etc. Furthermore, for $n \neq 1$, we would have a metal — although for the strong interaction $U \gg t$ it could be a special type of metal, still with strong correlations (such a metallic state could, in principle, be rather fragile and very sensitive and unstable to any extra perturbations — longer-range interactions, etc.). However, at least in the simplest case, this description catches the main physical effect: the creation of a novel state — a Mott insulator with localized electrons for half-filled bands (one electron per site: $n = 1$) and for the strong interaction $U/t \gg 1$. And one can see that in this state we simultaneously create localized magnetic moments: each electron localized at a respective site gives a localized magnetic moment, corresponding to $S = 1/2$.

When we take into account in this situation only the dominant term in Hamiltonian (3), the interaction term $Un_{i\uparrow}n_{i\downarrow}$, the spin direction would not matter, and the system would be paramagnetic (with disordered localized spins). However, if we also consider electron hopping, the first term in formula (3), this hopping lifts spin degeneracy in the second order of the perturbation theory in $t/U \ll 1$, thus leading to the antiferromagnetic interaction of localized spins $\sim t^2/U$, i.e., the low-lying energy states of the system can be effectively described by the Heisenberg model (see Section 3.2 for details)

$$H = J\sum_{ij}\mathbf{S}_i\mathbf{S}_j = \frac{2t^2}{U}\sum_{ij}\mathbf{S}_i\mathbf{S}_j\,, \tag{4}$$

where $\mathbf{S}_i$ is the spin operator acting at the site i, and J is the exchange coupling between spins at two such sites (and hence, in principle, it can be different for various pairs, i.e., $J \to J_{ij}$ in this situation). The ground state of the system under consideration would be a Mott insulator with antiferromagnetic spin ordering. For only two sites and two electrons, we would then arrive at the singlet ground state

$$\Psi_{\rm HL} = \frac{1}{\sqrt{2}}\left(c^{\dagger}_{1\uparrow}c^{\dagger}_{2\downarrow} - c^{\dagger}_{1\downarrow}c^{\dagger}_{2\uparrow}\right)|0\rangle\,. \tag{5}$$

This is what is called the Heitler–London (HL) description in the chemical bond theory.

It should be noted here that for noninteracting electrons described by the simple Hamiltonian (1) the ground state would also be a unique singlet state — a filled Fermi surface, in which there are two electrons with spins 'up' and 'down' in every occupied state. For only two such sites, the ground state would also be a singlet:

$$\Psi_{\mathrm{MO}} = \frac{1}{2}\left(c_{1\uparrow}^{\dagger} + c_{2\uparrow}^{\dagger}\right)\left(c_{1\downarrow}^{\dagger} + c_{2\downarrow}^{\dagger}\right)|0\rangle\,. \tag{6}$$

Such a state in the theory of chemical bonds is called the Hund–Mulliken state, or molecular orbital (MO) state (sometimes listed as MO LCAO: Molecular Orbital — Linear Combination of Atomic Orbitals).

In quantum chemistry, it was relatively soon realized that both MO (6) and HL (5) wave functions describe just two limiting cases, and for realistic calculations one should instead employ a linear combination of homeopolar states, given by the HL wave function (5) and ionic contributions $c_{1\downarrow}^{\dagger}c_{1\uparrow}^{\dagger} + c_{2\downarrow}^{\dagger}c_{2\uparrow}^{\dagger}$, but (in contrast to MOs) with a variational coefficient:

$$\Psi_{\mathrm{CF}} = \left[\frac{\sin\theta}{\sqrt{2}}\left(c_{1\uparrow}^{\dagger}c_{2\downarrow}^{\dagger} - c_{1\downarrow}^{\dagger}c_{2\uparrow}^{\dagger}\right) + \frac{\cos\theta}{\sqrt{2}}\left(c_{1\downarrow}^{\dagger}c_{1\uparrow}^{\dagger} + c_{2\downarrow}^{\dagger}c_{2\uparrow}^{\dagger}\right)\right]|0\rangle\,. \tag{7}$$

The wave function in the form Ψ_{CF} is often called the Coulson–Fisher wave function [14]. These notions will be very important for our discussion in the main body of this paper.

It is thus seen that the dichotomy between two descriptions of chemical bonds in molecules — MO and HL approaches — has exact counterparts in two types of solids: those with itinerant electrons described by the band theory, and localized electrons in Mott insulators possessing strong electron correlations. But, in contrast to the case of molecules, where with an increase in electron correlations we continuously go over from the MO to HL description [cf., for example, the Coulson–Fisher form (7)], for a large concentrated solid these two states are really two different thermodynamic states of matter with sharp, well-defined transition between them — the Mott transition. This transition can be caused simply by a change in the parameter U/t (which can in many systems be reached experimentally under pressure, which leads to an increase in electron hopping t, but in some very interesting cases also by a change in temperature, the level of doping, etc). And the properties of a system close to this localized–itinerant crossover turn out to be very interesting and nontrivial, with some rather unexpected features emerging (see Section 5.2).

3. Basic effects related to the orbital degrees of freedom

3.1 Crystal-field splitting, spin-state transitions

When we want to apply these general ideas to TM compounds, several important ingredients have to be included, which make the description, on the one hand, more realistic, but which, on the other hand, often lead to novel phenomena. The most interesting (from the point of view of physical properties) TM compounds have partially filled d-bands. Five d-states are degenerate in isolated atoms or ions, but become split when the ion is put into a crystal. In fact, these split states have to be classified according to corresponding irreducible representations. Thus, if a TM ion finds itself inside the ligand octahedra, as often happens in TM compounds (e.g., NiO, La_2CuO_4, $LaCoO_3$), its d-levels are split into the t_{2g} and e_g subshells: the e_g-orbitals are directed as much as possible towards the ligands, while the t_{2g} 'look' between them (Fig. 2). This effect is called crystal-field splitting.

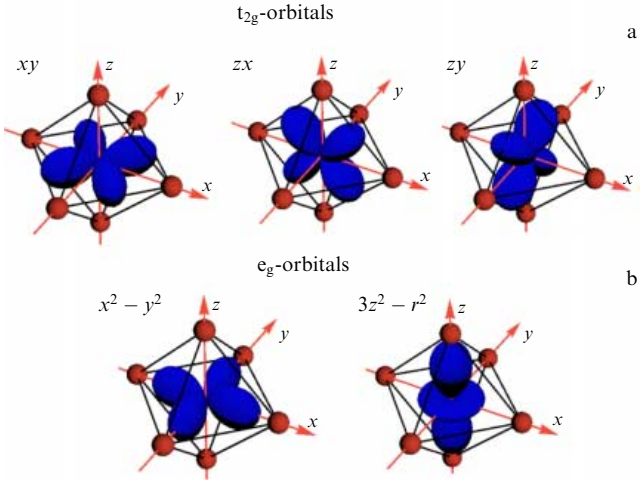

Figure 2. Cubic harmonics corresponding to d-orbitals in an octahedral surrounding.

There are two equally important contributions to crystal-field splitting. First of all, there is indeed an effect of the electric field created by a local surrounding. Negatively charged ligands repel a negative electron charge density corresponding to d-orbitals. This repulsion is larger for the e_g-orbitals directed toward the ligands, and these orbitals go higher in energy than the t_{2g} ones. However, there is also another contribution to the crystal-field splitting that is due to a hybridization of d-orbitals and the ligand p-orbitals. In conventional TM compounds, the ligand p-orbitals lie lower in energy than the d-orbitals of TMs, and the hybridization between them shifts the d-orbitals even higher. In the case of an octahedral surrounding, this shift will be larger for the e_g orbitals. So we see that both effects usually act one way.

However, there can be exceptions to this rule: for instance, if at least some of ligand p-states lie *higher* than d-orbitals, the hybridization will push these d-states down, while Coulomb forces push them up (both stronger for e_g orbitals). If hybridization wins, the bonding states of e_g symmetry (these will be a mixture of p- and d-orbitals) will be *lower* than those of t_{2g}. This happens in $Cs_2Au_2Cl_6$ [15], and it can also be expected in other systems with a negative charge-transfer gap, Δ_{CT}, which is the energy cost for the reaction[1] $d^n p^6 \rightarrow d^{n+1}p^5$. A negative charge-transfer regime can be realized in the case of an unusually high oxidation state of a TM, when a system cannot afford such a strong charge redistribution between a metal and a ligand, as the chemical formula requires. That is why the holes emerge in the ligand p-orbitals, which appear to be higher in energy than some of the d-orbitals in these systems. Thus, for example, in CrO_2, where Cr nominally possesses valence 4+ and O does 2−, it is rather unfavorable to transfer four electrons from the Cr ion to O;

[1] If $\Delta_{\mathrm{CT}} > 0$, as in normal TM oxides, we lose the energy transferred by electrons from a ligand to a transition metal, while if $\Delta_{\mathrm{CT}} < 0$, such a transfer occurs spontaneously to minimize the total energy of a system.

instead, holes appear in the O 2p-band, with Cr being practically 3+ [16].

The crystal-field splitting ($\Delta_{\rm CFS}$) often has a dramatic influence on the magnetic properties of TM compounds. We know from atomic physics that Hund's rules determine the ion state with partially filled levels. As a matter of fact, they say that the state of a many-electron system should be such that, first, the total spin $S_{\rm tot} = \sum_i s_i$, and then the total orbital moment $L_{\rm tot} = \sum_i l_i$ of an ion should take the maximum possible values. This, in particular, means that, e.g., a Co^{3+} ion with outer electron configuration $3d^6$ should have $S_{\rm tot} = 2$. However, this is not always the case. When a TM ion is implanted into an octahedral surrounding, the ligand crystal field splits its d-shell, making the filling of higher lying d-levels (e_g levels in the octahedra) energetically unfavorable, which may result in violation of first Hund's rule. A classical example of such a situation is $LaCoO_3$, where the spin state of Co^{3+} is the low-spin $S_{\rm tot} = 0$ (electron occupation t_{2g}^6), and the transition (known in chemistry as spin crossover) from the low-spin ($S_{\rm tot} = 0$, $t_{2g}^6 e_g^0$) to the intermediate-spin ($S_{\rm tot} = 1$, $t_{2g}^5 e_g^1$) or to a mixture of low-spin and high-spin ($t_{2g}^4 e_g^2$) states occurs [17–20].

It is often sufficient to describe Hund's rule in the mean-field approximation by the following Hamiltonian:

$$H_{\rm Hund} = -J_{\rm H} \sum_{m \neq m'} \left(\frac{1}{2} + 2 S_m^z S_{m'}^z \right), \qquad (8)$$

where m, m' numerate orbitals, and $J_{\rm H}$ is the intraatomic Hund's exchange parameter. It is easily seen that if one uses this Hamiltonian, then, in order to find the Hund's exchange energy for each atomic configuration, one needs simply to count the number of inequivalent pairs of electrons with parallel spins (e.g., for Co^{3+} the low-spin state will have $E_{\rm Hund} = -6J_{\rm H}$, intermediate-spin $E_{\rm Hund} = -7J_{\rm H}$, and high-spin state $E_{\rm Hund} = -10J_{\rm H}$).

Spin-state transitions can be found in many other TM compounds based, in addition to Co^{3+}, on Fe^{2+}, and more rarely on Fe^{3+}, Mn^{2+}, and Mn^{3+} ions. It is rather important to mention two points in this regard. First of all, spin-state transitions are more typical for 3d, not for 4d and 5d, TM compounds. In 3d systems, the $t_{2g} - e_g$ splitting is $\Delta_{\rm CFS} \sim 1.5-2$ eV and it can easily compete with the intra-atomic exchange interaction, which is given by $J_{\rm H} \sim 1$ eV and which arranges electrons according to Hund's rule. In contrast, due to a larger principal quantum number, the 4d and 5d orbitals are more spatially extended than the 3d ones [3]. As a result, both kinetic and Coulomb contributions to the crystal-field splitting are larger, and the $t_{2g} - e_g$ splitting exceeds 3–4 eV in systems based on these ions [21].

As a result, 4d and 5d elements typically adopt low-spin states, putting as many electrons as possible into the lower-lying t_{2g} levels. While one cannot completely rule out the possibility that even in this case spin-state transitions may occur within t_{2g} levels split by a noncubic crystal field, this is generally rather unlikely, since corresponding splitting is typically much smaller than $J_{\rm H}$. Indeed, attempts to describe the properties of some materials by the spin-state transition caused by crystal-field splitting of the t_{2g} subshell (see, e.g., Ref. [22]) have failed [23–25]. One might expect, though, that this idea may apply to some early 5d TM compounds, where $J_{\rm H}$ is expected to be rather small (0.3–0.5 eV) and $\Delta_{\rm CFS}$ within the t_{2g} subshell can also be ~ 0.5 eV due to the noncubic crystal field.

3.2 Orbital degrees of freedom and magnetism

While crystal-field splitting in the t_{2g} or e_g subshells (not the main splitting between t_{2g} and e_g!) is unlikely to lead to a spin-state transition, it (and more so the 'main' $t_{2g} - e_g$ crystal-field splitting) may greatly affect the magnetic properties of materials via a completely different mechanism. In strongly correlated systems, even small crystal-field splitting may result in electron localization on a particular orbital. Moreover, it turns out that the magnetic properties of a system strongly depend on the particular orbitals on which electrons are localized. There are the so-called Goodenough–Kanamori–Anderson (GKA) rules [3], which describe the relationship between the orbital occupation and the resulting magnetic coupling in systems with localized electrons. In describing these rules, we will employ the terminology of filled (two electrons), half-filled (a single electron), and empty orbitals, and will explain how these rules can be applied to most common geometries.

It is easier to start with a direct overlap between d-orbitals (*direct exchange*), and then consider a situation more typical for TM compounds, when TM ions are separated by ligands, so that the corresponding d-orbitals practically do not overlap directly with each other and all hopping processes occur via ligand p-orbitals (the so called *superexchange*).

Direct exchange. Case 1: *the exchange coupling between two overlapping half-filled orbitals is strong and antiferromagnetic.*

This situation is illustrated in Fig. 3a. In the limit of large Hubbard repulsion, $U \gg t$, electrons are mostly localized on TM sites. If two electrons have different spin projections, i.e., are AFM coupled, they can sometimes hop from site to site and gain some kinetic energy. One may easily evaluate a correction to the ground-state energy due to this hopping, using second-order perturbation theory with respect to t/U: $\delta E_{\rm AFM} = -2t^2/U$. Factor 2 appears here since both electrons can hop. U is the energy of an intermediate perturbed state (when both electrons are on the same site) with respect to the ground-state energy E_0. In the opposite situation of FM-coupled spins, electrons cannot hop due to the Pauli principle and do not display this energy gain. Thus, the exchange integral becomes AFM (positive):

$$J_1 = E_{\rm FM} - E_{\rm AFM} = E_0 - \left(E_0 - \frac{2t^2}{U} \right) = \frac{2t^2}{U} \qquad (9)$$

(compare with formula (15)).

Direct exchange. Case 2: *the exchange coupling between overlapping half-filled and empty orbitals is weak and turns out FM.*

First of all, since only one half-filled orbital can be directed along the line connecting two sites (otherwise there

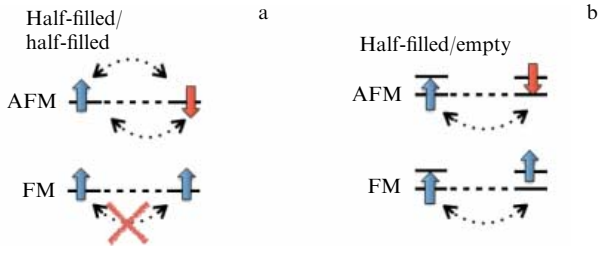

Figure 3. Sketch illustrating hopping processes in the case of a direct overlap between (a) two half-filled and (b) half-filled and empty d-orbitals.

will be overlap between these two half-filled orbitals), only one electron can hop from site to site, and hence there will be no factor 2 in the expression for the exchange integral. Second, the Pauli principle does not restrict in this case any hoppings, and both AFM- and FM-coupled ions gain some energy due to these processes (Fig. 3b). However, it can be seen that this gain will be larger for FM, since the energy of the excited (virtual) state with two electrons on the same site in this case is smaller — this state follows Hund's rule: both electrons have the same spin and hence the energy of this state is $U - J_H$, and not U, as it was for AFM. The corresponding exchange parameter becomes FM (negative):

$$J_2 = E_{FM} - E_{AFM} = E_0 - \frac{t^2}{U - J_H} - E_0 + \frac{t^2}{U} \sim -\frac{t^2 J_H}{U^2} \tag{10}$$

(for $J_H < U$, which is almost always the case). This result can also be used for the case of overlap between (completely) filled and half-filled orbitals: one should just consider holes instead of electrons.

It is worthwhile to note that for 3d TM ions $J_H \sim 1$ eV, while $U \sim 5-7$ eV [1]. Therefore, $|J_2|$ is usually (much) smaller than J_1, as defined by Eqn (9). This simple result has rather general consequences. We see that in insulators the FM contributions to the exchange coupling are generally much smaller than the AFM ones: $J_1/|J_2| \sim U/J_H$. This is the reason why most of the insulating TM compounds with localized electrons appear as AFM, not FM (in contrast to metals, which are typically FM). There must be special conditions which allow FM J_2 to overcome J_1 (like small U, a specific geometry, or a particular filling of d-levels, which switches off the AFM contribution). Moreover, even if the FM contribution dominates, the resulting Curie temperature is usually much smaller than the Néel temperature in AFM. Thus, for example, the antiferro-orbital ordering (leading, for example, to overlap between half-filled and empty orbitals) does stabilize FM in $YTiO_3$, but $T_C \sim 30$ K, while in the AFM $LaTiO_3$ the ferro-orbital ordering (overlap of half-filled with half-filled orbitals) results in $T_N \sim 150$ K [26–28]. The Curie temperatures in ferromagnetic $NaCrGe_2O_6$ ($T_C \sim 6$ K [29]) and in Ba_2NaOsO_6 ($T_C \sim 7$ K [30]) are much less than the typical values of Néel temperatures in AFM TM oxides.

A word of caution should be mentioned with respect to Eqns (9) and (10), which were derived for the cases of only one electron and two electrons per site, (9) and (10), respectively. In real materials the occupation of d-states can be very different, and these formulas must be rewritten accordingly. One needs to calculate the energy of the intermediate state accurately. For example, in the case of three electrons per site and a half-filled/half-filled overlap between one of the orbitals, $J_1 = 2t^2/(U + 2J_H)$: in the initial state the hopping electron experiences Hund's rule 'attraction' to the other two electrons at this site; this energy is lost in the (virtual) intermediate state when this electron is transferred to a neighbor.

Also, in writing down the expressions for different exchange constants, we used the same value of U for different orbital occupations. In fact, this interaction is different for two electrons on the same (U) and on different (U') orbitals. In the t_{2g} subshell, one can make use of the so-called Kanamori parameterization [31]: $U' = U - 2J_H$; and in general, one has to employ the full atomic description, using Racah parameters A, B, and C [32]. This can change the exact expressions and numerical values of exchange constants, but the general qualitative rules formulated by Goodenough, Kanamori, and Anderson (GKA rules) remain valid.

Up to now, we have discussed direct overlap between d-orbitals. However, this situation is rather atypical for TM compounds, where TM ions are usually separated by ligands and are often quite far away from each other. Since d–d hopping scales as [33, 34]

$$t_{dd} \sim r^{-(2l+1)} \sim r^{-5}, \tag{11}$$

where r is the distance between TM ions, the direct exchange interaction is often rather inefficient. In this situation, the electron hopping occurs via the ligand p-orbitals (superexchange). General rules governing the overlap between filled, half-filled, and empty orbitals remain valid, but the analysis becomes more complicated, since one also needs to take into account, in addition to d-states, the energetics related to the ligand orbital and all various exchange paths which these orbitals provide.

Here, we will consider in detail only the simplest situation of superexchange interaction between two half-filled d-orbitals via the p-orbital, as shown in Fig. 4a (see Ref. [1] for a more complete analysis). In this case, d-electrons will hop via ligand p-orbitals; corresponding hopping amplitudes are designated as t_{pd}. There are two possibilities for their implementations, as shown in Fig. 5. While the

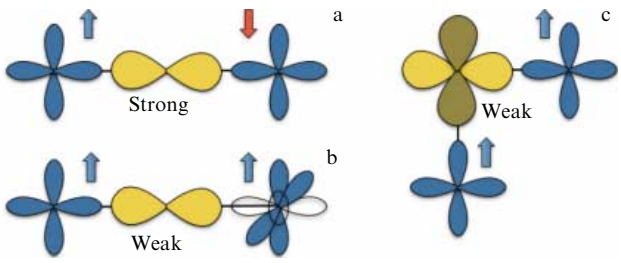

Figure 4. (Color online.) Three main types of superexchange interaction: (a) AFM superexchange between two half-filled d-orbitals via the same p-orbital; see Eqn (15); (b) FM superexchange between half-filled and empty d-orbitals via the same p-orbital; see Eqn (16), and (c) FM superexchange between two half-filled d-orbitals via different p-orbitals, see Eqn (17); d-orbitals of the TM ions are shown in blue (half-filled) and white (empty), while ligand p-orbitals are in yellow. In this figure, only the e_g orbitals are considered; corresponding plots for the t_{2g} orbitals can be found, e.g., in Ref. [35].

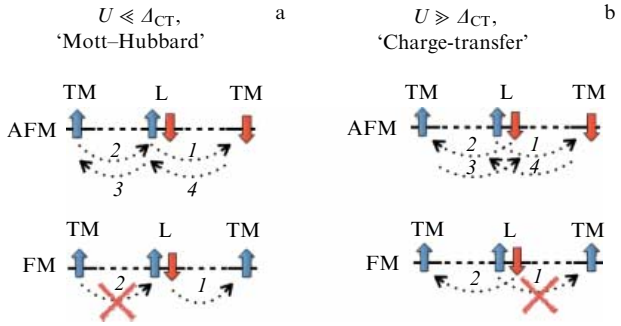

Figure 5. Schematic illustration of the hopping processes in superexchange interaction between half-filled orbitals in two regimes: (a) Mott–Hubbard regime, and (b) charge-transfer regime (L stands for a ligand, and TM labels a transition metal ion). The hopping order is designated by numbers *1–4*.

energy of the excited state after the first such hop is the same, viz. Δ_{CT}, the hopping processes at steps 2 and 3 are different.

If Hubbard's U is smaller than the charge transfer energy Δ_{CT}, $U \ll \Delta_{CT}$, then at step 2 we move the d-electron to the vacant place in the p-shell (the energy of this state is U), and with processes 3 and 4 we restore the *status quo*. The corresponding expression for the exchange constant reads as follows:

$$J \sim \frac{t_{pd}^4}{\Delta_{CT} U \Delta_{CT}} = \frac{\left(t_{dd}^{eff}\right)^2}{U} . \tag{12}$$

Here, we have intentionally introduced the effective d–d hopping integral via p-orbitals:

$$t_{dd}^{eff} = \frac{t_{pd}^2}{\Delta_{CT}} , \tag{13}$$

to demonstrate that the superexchange interaction in this case has exactly the same form as the direct exchange defined previously [see formulas (4), (9)].

In the opposite limit of $U \gg \Delta_{CT}$, it is easier to move at the second step the second electron from a ligand to another TM ion. In this case, one has

$$J \sim \frac{t_{pd}^4}{\Delta_{CT}(\Delta_{CT} + U_{pp}/2)\,\Delta_{CT}} = \frac{\left(t_{dd}^{eff}\right)^2}{\Delta_{CT} + U_{pp}/2} . \tag{14}$$

Here, U_{pp} is the on-site Coulomb repulsion of two holes in the p-shell of a ligand (it also takes into account the intraatomic exchange).

The $U \ll \Delta_{CT}$ limit corresponds to Mott–Hubbard insulators, while $U \gg \Delta_{CT}$ corresponds to charge-transfer insulators. However, U and Δ_{CT} in many real materials can be of the same order of magnitude, and one needs to take into account both contributions:

$$J \sim \left(t_{dd}^{eff}\right)^2 \left(\frac{1}{U} + \frac{1}{\Delta_{CT} + U_{pp}/2}\right) . \tag{15}$$

Without further details, we list below the dominant contributions to the exchange interaction for three main geometries: when two neighboring MO_6 octahedra share their corners, edges, and faces (Fig. 6).

Common corner. Typical crystal structures with this geometry are perovskites (normal, double, quadruple, and layered). Since there is a ligand (L) between TM ions, the dominating exchange interaction will be the 180° superexchange (15). The AFM exchange between half-filled e_g orbitals via the σ(p–d) bond characterized by the hopping integral $t_{pd\sigma}$ appears as the strongest (Fig. 4a). In addition, there can also be a moderate AFM superexchange between half-filled t_{2g} orbitals via the same p-orbital (described by the same expression (15)), since π bonding is much weaker than σ ($t_{pd\sigma} \approx 2t_{pd\pi}$ [34]). The last contribution is a weak FM exchange between half-filled and empty *d*-orbitals (Fig. 4b):

$$J \sim -\left(t_{dd}^{eff}\right)^2 \left(\frac{J_H}{U^2} + \frac{J_H}{(\Delta_{CT} + U_{pp}/2)\,\Delta_{CT}}\right) . \tag{16}$$

Common edge. Typical materials with such crystal structures involve pyroxenes, delafossites, spinels (AM_2L_4), and hexagonal '213' systems ($(Li, Na)_2MO_3$) (see also Sections 4.3 and 6.5 for a detailed discussion). There is a substantial direct d–d overlap of two half-filled t_{2g}-orbitals (Fig. 6b), which will result in a strong AFM exchange (9). There will also be a 90° superexchange interaction:

— first of all, a moderate AFM exchange appears via the same p-orbital (see Fig. 28) (one can use formula (15) with the appropriate choice of t_{pd} in this case);

— second, there is also an FM superexchange between half-filled and empty d-orbitals, which is shown in Fig. 4 of Ref. [35] and which can be described by expression (16);

— finally, there is also a possible FM superexchange between two half-filled e_g- (or t_{2g}-) orbitals via two different p-orbitals, as shown in Fig. 4c (for the t_{2g}-orbitals, see Fig. 5 of Ref. [35]):

$$J \sim -\frac{\left(t_{dd}^{eff}\right)^2 J_H^p}{(\Delta_{CT} + U_{pp}/2)\,\Delta_{CT}} , \tag{17}$$

where J_H^p stands for the Hund's intraatomic exchange interaction on the ligand site.

Common face. Typical crystal structures are one-dimensional or dimerized systems such as $BaRuO_3$, $CsCuCl_3$, or 6H-perovskites with the general formula $Ba_3(M1)(M2)_2O_9$ (where $M1$ and $M2$ are metals), etc. It is believed that the strongest exchange coupling will be between the a_{1g}-orbitals ($a_{1g} = (xy + yz + zx)/\sqrt{3}$ in the local coordination system, where axes are directed towards ligands) (Fig. 6c). This contribution will be exceptionally large for 4d and 5d TM ions, the wave functions of which are more spatially extended than 3d. Such an exchange is strong and AFM. It is interesting to note that the spin–orbit (Kugel–Khomskii) Hamiltonian describing the interplay between spin and orbital degrees of freedom has, in this case, unusually high symmetry — SU(4) [36, 37].

To end this section, we would like to note that, in principle, there can be exchange processes via not one but several intermediate ions. Sometimes this exchange interaction is referred to as a supersuperexchange [38–40].

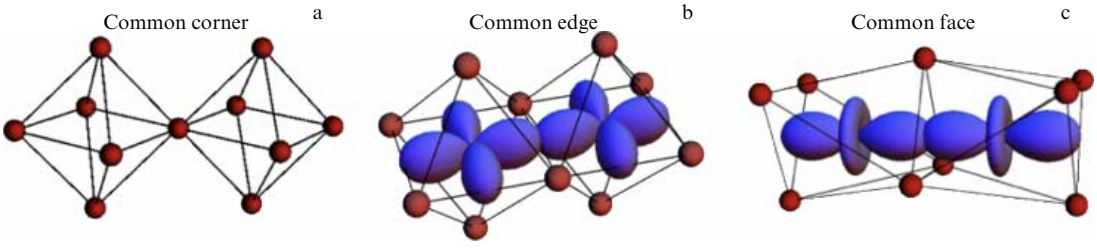

Figure 6. (Color online.) Three types of octahedra packing in TM compounds: for the common corner (a), for the common edge (b) and common face (c) cases; we also show d-orbitals with the largest direct overlap in figures (b) and (c). Ligands are shown as brown balls.

3.3 Double exchange

Let us turn to the exchange interactions in metals. We do not consider all metals, but only those in which local magnetic moments still exist. Moreover, we examine a situation when there are two sets of electrons — one providing localized magnetic moments, and the other giving metallic conductivity. In some sense, this is an extreme situation, since in conventional metals the same electrons can simultaneously be mobile and provide magnetic moments. But in many materials, like manganites [41], this is indeed a very good approximation: part of the electrons are localized (due to strong Hubbard U), while the other (metallic) electrons can be added to a system, e.g., by doping. One can assume that these two types of electrons interact with each other via intra-atomic Hund's exchange $J_{\rm H}$:

$$H = -t\sum_{\langle ij\rangle\sigma} c^{\dagger}_{i\sigma}c_{j\sigma} - J_{\rm H}\sum_{i}\mathbf{S}_i\, c^{\dagger}_{i\sigma}\boldsymbol{\sigma}\, c_{i\sigma} + J\sum_{\langle ij\rangle}\mathbf{S}_i\mathbf{S}_j\,. \qquad (18)$$

Here, $\boldsymbol{\sigma}$ is the vector of Pauli matrices, while σ is the spin. The first term gives a band spectrum of mobile electrons (described by operators $c^{\dagger}_{i\sigma}, c_{j\sigma}$); the second one introduces the coupling between mobile and localized electrons (with spin $\mathbf{S}_i$). The last term describes an exchange coupling between localized spins of neighboring sites.

In the case of small doping, all mobile electrons are at the bottom of a band, the width W of which is defined by the hopping integral t and the number of nearest neighbors z: $W \sim 2zt$. Thus, we can lower the total energy of a system considerably (by $\sim xW/2$, where x is the concentration of mobile electrons), if mobile electrons propagate through the lattice. However, if localized spins are AFM-ordered, the intraatomic Hund's exchange prevents (or at least strongly suppresses) such a propagation, since there are sites at which the spins of mobile and localized electrons would be antiparallel (Fig. 7). Thus, to gain kinetic energy of mobile electrons, it is better to make the system ferromagnetic. We see that, in contrast to direct exchange and superexchange discussed in items *2* and *3* of Section 3.2, this mechanism, called *double exchange* in the literature, tends to stabilize ferromagnetism. The corresponding model, given by formula (18) (sometimes omitting the second term, with the assumption that $J_{\rm H}$ is much larger than the other parameters of the system), is called the double exchange (DE) or ferromagnetic Kondo lattice model. Other details of this mechanism and a more detailed treatment of the model can be found in review [42] and in original papers [43–47]. Here, we would like to mention just a couple of points.

First of all, let us give some examples of systems where the DE operates. These include manganites, such as $La_{1-x}Sr_xMnO_3$, where electrons in the narrow t_{2g} band are considered to be localized (and to have local magnetic moments). By doping, one may add some holes or electrons to the much wider e_g band. The electrons or holes in the e_g band play the role of itinerant carriers [43]. Another example is CrO_2, where we do not need doping to 'switch on' the DE. There are localized electrons in the xy band, which provide local magnetic moments, and itinerant electrons in the xz/yz bands, which make the system ferromagnetic by hopping from site to site [16].

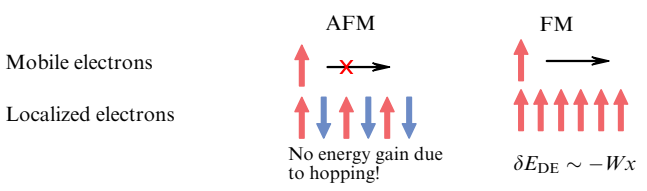

Figure 7. Sketch illustrating the double exchange mechanism of ferromagnetism.

Second, there can be a conventional direct or superexchange interaction between localized spins, described by the last term in Eqn (18), which is usually AFM, as explained in Section 3.2. The competition between the AFM superexchange and the FM double exchange can result in a canted magnetic state with the angle θ between neighboring spins, $\cos(\theta/2) \sim tx/(4JS^2)$ [46] for appropriate concentration x of conduction electrons (see also the discussion in Refs [47, 48]). Another more plausible option implies that for small doping there may appear in a system, instead of homogeneous canting, a phase separation into the undoped antiferromagnetic matrix and ferromagnetic droplets containing all doped electrons [49]. There are experimental indications that such phase separation indeed exists in low-doped manganites [50].

Finally, there is an important question as to what happens with the double exchange, if a small band gap appears, which prevents propagation of itinerant electrons. Or, in other words, how the double exchange concept could be combined with the superexchange picture in a multiorbital case. While this problem is still not completely solved, it was recently shown that the double exchange survives even in the insulating regime, if $J_{\rm H}$ is large enough [51, 52]. Moreover, for a certain range of parameters, a phase appears with partially suppressed total magnetization. It is clear that the natural generalization of the double exchange model would lead to a picture which retains differentiation of electrons on more localized and more itinerant, but which does not require metallic conductivity. Obviously such a difference can be provided by a spatial ordering of corresponding orbitals. In Section 5.2, we will discuss for the example of dimerized systems the interplay between the orbital-selective behavior and magnetic properties, in particular, the eventual suppression of double exchange by the formation of orbital-selective 'molecular' states.

3.4 Jahn–Teller effect

Yet another important factor which we should mention here is that for certain types of symmetry and for some d-electron occupations we can have an extra orbital degeneracy. This is the case, for example, for TM ion having four d-electrons, all with spin 'up' (Mn^{3+} or Cr^{2+}) in the octahedral coordination. Three electrons occupy the t_{2g} levels, which are half-filled, and the fourth electron then goes over into the e_g state. But for regular octahedra, these e_g levels are doubly degenerate. Thus, this extra electron can occupy any of these states: $3z^2 - r^2$, $x^2 - y^2$, or any of their linear combinations. This leads to the well-known instability, known as the Jahn–Teller (JT) effect: it is favorable to reduce the symmetry of a system, e.g., distort the initially regular O_6 octahedron around the TM ion in an oxide, leading to the splitting of d-levels and to some gain in energy.

Such splitting for the tetragonal elongation of an O_6 octahedron is shown in Fig. 8a. It is clearly seen that such a distortion splits the e_g levels, so that our fourth electron can now occupy the lowest e_g level and can decrease the total energy of the system. This decrease turns out to be linear in distortion u, i.e., $\delta E_{\rm kin} \sim -gu$, as the level splitting in a

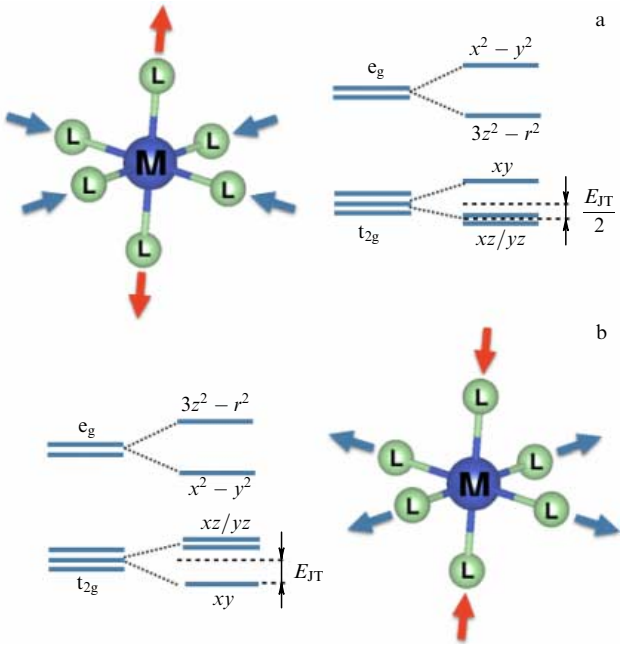

Figure 8. Tetragonal elongation (a) and compression (b) of a ligand (L) octahedron surrounding a metal ion (M), and corresponding splitting of the d-levels. In order to keep the volume of the crystal constant, the elongation (compression) along one of the axes is accompanied by compression (elongation) along two others.

Zeeman effect. Here, g is a parameter characterizing the coupling between an electronic subsystem and a lattice, and u is a strain. Of course, this distortion leads to an elastic energy loss, which, however, is only quadratic in the displacement: $\delta E_{\text{elast}} \sim Bu^2/2$ (B is the elastic modulus). The linear electronic energy gain always wins, and the minimum energy will be reached for a finite distortion: in this case, $u = \pm g/B$. This is, in simple terms, the essence of the JT theorem (which, according to Teller himself, was first suggested to him by Landau (see Appendix A.2 in monograph [1]).

For isolated centers, the Jahn–Teller instability leads to very interesting quantum effects, including the geometric (Berry) phase (which actually first appeared in the literature just in this context [53], long before the famous work by Sir M Berry). But for us, it is more important that for concentrated solids we can get in this situation structural phase transitions with corresponding orbital ordering (see, e.g., review [7]). Moreover, it is not clear what comes first — the JT distortions followed by orbital ordering, or vice versa. Indeed, in addition to the electron–phonon mechanism of the JT effect described above, there is another mechanism of orbital ordering, the so-called superexchange (or Kugel–Khomskii) mechanism [7]. We have already found out that a system may gain an exchange energy by setting up some orbital ordering [e.g., by occupying the overlapping half-filled orbitals, we gain an energy proportional to that given by Eqn (15)], and the crystal lattice will react to this by corresponding (JT) distortions. Sometimes, instead of a real orbital ordering in an undistorted high-temperature phase, we can speak about short-range orbital correlations.

Band structure calculations show that an orbital ordering can appear even in the absence of JT distortions, just due to the superexchange mechanism, and if we then allow lattice relaxation, the lattice will relax to the JT-distorted structure (in the LDA + U [54], [2] i.e., including electronic correlations described by Hubbard's U, which are needed to localize electrons on particular orbitals) [55, 56]. The more sophisticated LDA + DMFT calculations, [3] however, show that both the electron–phonon and the superexchange mechanisms are important, and they together determine the temperature of the JT transition [57–59]. We will not discuss this large and very interesting field here; but in dealing with real systems with orbital degeneracy, one always has to keep in mind the possibility of JT distortions, which could result in the formation of orbital ordering.

3.5 Spin–orbit coupling

When dealing with the TM compounds, especially with 4d and 5d TMs, one also has to take into account the real (relativistic) spin–orbit coupling (SOC), in these systems it becomes large comparable to many other parameters, especially for 5d compounds. Still, usually the spin–orbit constant λ (~ 0.5 eV for ions such as Ir, Pt) is smaller than the $t_{2g} - e_g$ crystal-field splitting Δ_{CFS}, which for 5d oxides is typically $\sim 3-4$ eV. For e_g electrons, the crystal field quenches the orbital moment and the SOC. Therefore, we should only expect strong effects of the SOC for systems with partially filled t_{2g} subshells. But most 4d and 5d compounds actually belong to such systems, since 4d and 5d TM ions usually occupy the low-spin state (see Section 3.1).

For the t_{2g} subshell with triply degenerate orbitals, one can, by applying the Wigner–Eckart theorem, describe orbitals using the equivalent orbital moment $l_{\text{eff}} = 1$. Indeed, matrix elements of the orbital moment for three t_{2g} orbitals coincide with those for $l = 1$ up to the sign of the spin–orbit constant [60]. In the following, we will use this very convenient language to describe 4d and 5d orbitals and for simplicity often omit the 'eff' subscript. One has only to take care of the magnitude and the sign of the effective spin–orbit coupling λ_{eff}, when it is written out for this effective moment.

Two remarks have to be made right away. The first is that, when we include the SOC, the electron–hole symmetry existing for the t_{2g} shell is broken. Without the SOC, the properties of systems containing one and five t_{2g} electrons, and also two and four of them, are equivalent with the electron–hole substitution. Therefore, one can easily 'translate' the results obtained, for example, for one electron to those with five electrons (or one hole) in the t_{2g} subshell. This, however, is no more the case in the presence of a (strong) SOC.

The second point is the way we consider the SOC in many-electron atoms or ions. In principle, it is a complicated, many-particle problem. A detailed analysis of the structure of atomic electronic terms, with real atomic parameters (Racah parameters A, B, and C, or intraorbital and interorbital Hubbard repulsion parameters U and U', and Hund's interaction J_{H}) is described, for example, in Refs [32, 60]. Generally, in atomic physics, one usually considers two limits, or two approximations. From the Dirac equation, one gets the SOC for one electron, $\zeta l_i s_i$ [61], with the positive coupling constant ζ (and dependent on the atomic number; see below). For many-electron atoms or ions with a relatively weak SOC (weaker than Hund's rule intraatomic exchange), one usually applies the LS or Russel–Saunders approximation. In this case, according to Hund's first rule (see, e.g., Ref. [1]), one

[2] LDA — local density approximation.
[3] DMFT — dynamic mean-field theory

first forms the total spin $\mathbf{S} = \sum_i \mathbf{s}_i$ and the total orbital momentum $\mathbf{L} = \sum_i \mathbf{l}_i$, and then invokes the spin–orbit interaction for these total moments:

$$H_{\mathrm{SOC}} = \lambda \mathbf{L}\mathbf{S}\,. \tag{19}$$

The energy contribution due to the SOC can be expressed via the total momentum $\mathbf{J}$ defined as $\mathbf{J} = \mathbf{L} + \mathbf{S}$:

$$E_{\mathrm{SOC}} = \langle \lambda \mathbf{L}\mathbf{S} \rangle = \frac{\lambda}{2}\left(J(J+1) - L(L+1) - S(S+1)\right),$$

since $\mathbf{J}^2 = \mathbf{L}^2 + \mathbf{S}^2 + 2\mathbf{L}\mathbf{S}$. The SOC constant is then given by $\lambda = \pm\zeta/(2S)$, where one takes plus for the less-than-half-filled shells, and minus for the more-than-half-filled shells. This finally leads to the second (or third) Hund's rule: for the less-than-half-filled shells ($\lambda > 0$), we have a normal order of multiplets (the terms with the smaller J have lower E_{SOC}), and an 'inverted' multiplet order (the lowest multiplets are those with the maximum J) for the more-than-half-filled shells.

When dealing with the effective moment $l = 1$ and the effective SOC for the t_{2g} shell, the sign of λ turns out to be the opposite [1, 60], so that we have a reversed multiplet order: multiplets with the larger J lie lower in energy for the less-than-half-filled t_{2g} shells, and we have a normal order for the more-than-half-filled shells. It is this factor that finally gives rise to an electron–hole asymmetry for this case. Thus, according to these rules, for a d^1 configuration, with $L = 1$ and $S = 1/2$, the possible values of the total momentum are $J = 1/2$ and $J = 3/2$, and according to the rules formulated above the lowest multiplet is the quartet $J = 3/2$. However, for five d-electrons (one hole in the t_{2g} shell), the multiplet order will be inverted, so that the ground state of such an ion would be a doublet $J = 1/2$. This is the state often invoked nowadays for compounds containing Ir^{4+} (t_{2g}^5) (see discussion below).

This treatment is applicable to light elements, with a relatively weak SOC. In the opposite limit of a very strong SOC, realized, for example, in rare earths or in actinides, another approximation is usually used — the so-called *jj*-coupling scheme (realized if the SOC constant λ is larger than Hund's exchange energy J_{H}). In this scheme, we first couple for each electron its spin and angular momentum to the total momentum of an electron:

$$\mathbf{j}_i = \mathbf{l}_i + \mathbf{s}_i\,, \tag{20}$$

and then form the total momentum out of those momenta for individual electrons:

$$\mathbf{J} = \sum_i \mathbf{j}_i\,. \tag{21}$$

In this scheme, a strong SOC splits the one-electron d-state into $j = 5/2$ and $j = 3/2$ components, and then the other interactions may remove the degeneracy of these levels. Note that, by doing this, we violate first Hund's rule, first of all taking care of the spin–orbit coupling (assumed to be stronger than Hund's exchange). A general schematic of d-level splittings in the presence of a crystal field and SOC is demonstrated in Fig. 9.

The 3d-compounds are definitely better described by the *LS* (Russel–Saunders) coupling scheme, and probably so are most 4d systems. But with 5d materials, the situation is not so clear. It might be that they are already 'half-way' between the *LS*- and *jj*-couplings.

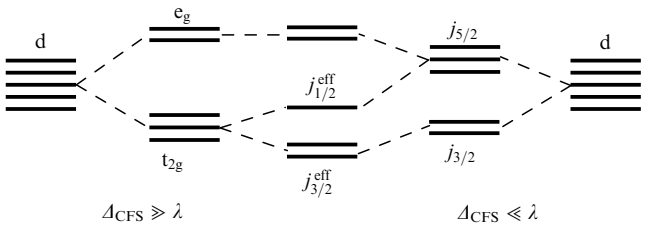

Figure 9. Schematic illustration of level splitting in the presence of cubic crystal field (CF) and of spin-orbit coupling.

For some d counts, these two pictures give qualitatively similar results, but for some others the conclusions might be different. Thus, for example, for the low-spin d^4 configuration in the *LS*-scheme $L = 1$, $S = 1$, and the ground state should be singlet $J = 0$. The same conclusion would be reached in the *jj*-scheme. In this scheme, we have single-particle states in the form of a low-lying $j = 3/2$ quartet and higher-lying $j = 1/2$ doublet (see Fig. 10). Four d-electrons would then occupy all states of the 3/2 quartet, i.e., the total J would also be zero.

The same is true for the most widely discussed case of d^5 occupation, as in Ir^{4+} ions. In the *LS* coupling scheme, as mentioned above, we would have $L = 1$, $S = 1/2$, and the ground state would be a Kramers doublet with $J = 1/2$. In the *jj*-scheme, we should fill the levels shown in Fig. 10 with five electrons, which would completely fill the lowest quartet, and the fifth electron would be in the $j = 1/2$ doublet, as in the *LS*-scheme. But, for example, the situation would be different for d^3 occupation. In the *LS*-scheme, these three electrons would fill all t_{2g} levels (the high-spin state), so that the net orbital momentum would be $L = 0$, and what remains would be a pure spin $S = 3/2$ state, without any influence of the SOC. In the *jj*-scheme, we also would have three electrons in a quartet, however not an $S = 3/2$ quartet, but a $j = 3/2$ quartet (Fig. 10). Consequently, the form of corresponding wave functions, the values of *g* factors, etc., would be different (see, e.g., Ref. [62]). Very recently, these effects were indeed observed for $5d^3$ systems Ca_3LiOsO_6 and Ba_2YOsO_6 [63].

It is also worth mentioning that all the band structure calculations based on the density functional theory (DFT) [64] are, in fact, dealing with one-electron states (one Slater determinant). In this sense, they describe the SOC in the

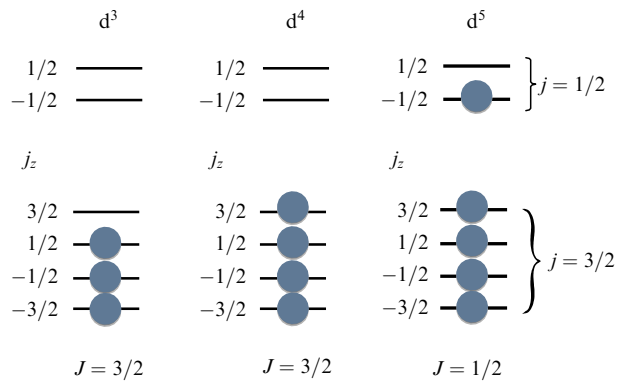

Figure 10. *jj*-scheme for d^3, d^4, and d^5 configurations (it is assumed that the $t_{2g} - e_g$ crystal-field splitting is large, so that all electrons occupy the t_{2g} levels).

jj-scheme, which also operates with one-electron states, before combining them into a total J state. In addition, experimentalists very often use the description with energy schemes similar to Fig. 10. One has to realize, though, that the real atomic electronic terms, real multiplets, are many-particle states, especially in the *LS*-coupling scheme.

One more comment is in order here. We have said above that the SOC becomes stronger with increasing atomic number Z of an element, and it is due to this fact that the heavier elements like 5d TM may already be close to the *jj*-coupling scheme. Very often in the literature, the estimate is given that the spin–orbit coupling constant $\lambda \sim Z^4$, where Z is the atomic number of an element; this has already become an accepted notion. But in the famous textbook [61], it is shown that in fact this relation should instead be $\lambda \sim Z^2$, not Z^4 [61]! And, indeed, a comparison with the experimental data demonstrates that this estimate is much closer to reality (though both are, of course, 'order-of-magnitude estimates'). For example, compare Ir and V. Ir has atomic number $Z = 77$ and $\lambda = 400$ meV [65]. V has atomic number $Z = 23$ and $\lambda \sim 30$ meV [60]. In effect, $\lambda_{Ir}/\lambda_V = 13.3$. Now, the 'Landau estimate' gives $(Z_{Ir}/Z_V)^2 = 11.2$, but the more commonly used 'rule' $\lambda \sim Z^4$ would give $(Z_{Ir}/Z_V)^2 = 125$ — way off! Thus, it seems that the dependence $\lambda \sim Z^2$ is indeed a correct one.

4. Effective reduction of dimensionality due to orbital degrees of freedom and its consequences

The original investigations of 'orbital physics' in solids were mostly concentrated on the study of the effects connected with orbital degeneracy and with the resulting phase transitions — the cooperative JT effect, or orbital ordering (these terms actually denote the same phenomenon, just stressing different aspects of it). These effects have been discussed in many books and review articles, e.g., Refs [7, 78, 79]. Later on, some novel aspects of orbital physics have attracted significant attention and come to the forefront.

In the present review, we will mostly concentrate on this novel developments; the older, more 'classical' parts of this field can be found in the literature cited above.

We start by discussing the phenomenon which was highlighted relatively recently and which was shown to lead to many interesting consequences. This is the reduction of the effective dimensionality of electronic and magnetic subsystems, which is the result of the directional character of d-orbitals (see, e.g., Fig. 2). We will describe these effects with several examples, before formulating general conclusions. In Table 1, we give a list (far from complete!) of several materials in which the phenomenon of reduction of effective dimensionality has been examined both experimentally and theoretically.

Table 1. Examples of materials with an effective reduction of the dimensionality due to orbital degrees of freedom.

Type of reduction	Materials	References
1D → 0D, zigzag chains → dimers, $S=0$	$NaTiSi_2O_6$	[35, 66]
1D → 0D, chains → dimers	TiOCl	[67]
2D → 0D, triangular layers → isolated triangles ($S=0$)	$LiVO_2$	[68, 69]
3D → 0D, spinel → heptamers, $S=0$	AlV_2O_4	[70, 71]
3D → 0D, spinel → octamers, $S=0$	$CuIr_2S_4$	[72, 73]
3D → 1D, spinel → tetramerized chains ($S=0$)	$MgTi_2O_4$	[73, 74]
3D → 1D, 3D-perovskite → AFM-chains $S=1/2$	$KCuF_3$	[75, 76]
3D → 1D, 3D-pyrochlore → Haldane chains	$Tl_2Ru_2O_7$	[77]

4.1 Formation of low-dimensional magnetic systems due to orbital ordering

The simplest example, known already long ago, is the formation of low-dimensional magnetic systems in materials which just by the crystal structure belong to the usual three-dimensional ones. Probably the most striking example is $KCuF_3$. The latter is an insulating perovskite, with basically a cubic lattice, containing classical JT ions Cu^{2+} ($t_{2g}^6 e_g^3$), with one hole in doubly degenerate e_g orbitals. Due to electron–lattice (JT) interaction [78] and the superexchange mechanism [7, 75], an orbital ordering with the (half-filled) hole orbitals occurs in $KCuF_3$ as illustrated in Fig. 11 (the half-filled hole orbital of the $x^2 - y^2$ type is shown).

Remembering the GKA rules discussed in Section 3.2, we expect that in this system a strong antiferromagnetic exchange should exist along the *c*-direction, in which these orbitals strongly overlap (via corresponding p-orbitals of F). The coupling in the *ab* plane is ferromagnetic and much weaker: the half-filled orbitals here are orthogonal to each other, and there is an overlap only between half-filled and completely filled (in the electron picture) or between half-filled and empty (in the hole representation) orbitals. And, indeed, the magnetic properties of $KCuF_3$ ideally correspond to these expectations: this system turns out to be a quasi-one-dimensional antiferromagnet, with weak ferromagnetic coupling between these AFM chains, which finally leads to A-type long-range magnetic ordering [FM layers stacked antiferromagnetically (see Fig. 11)]. Thus, in effect, this material, which is crystallographically cubic, turns out to be magnetically one of the best 1D antiferromagnets known [76]! And

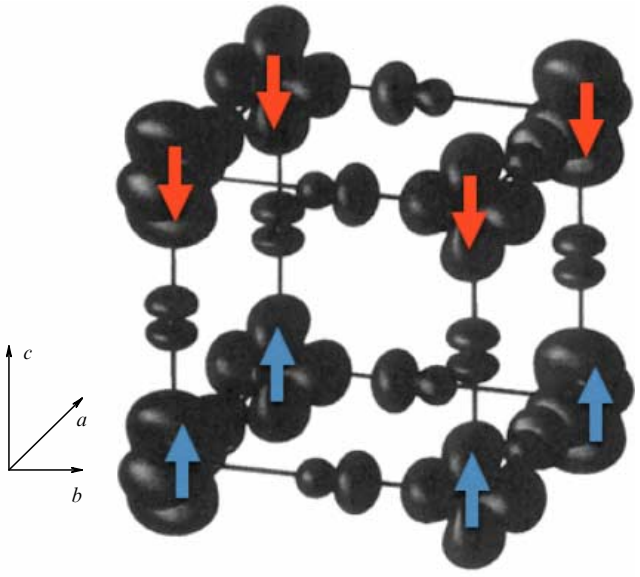

Figure 11. Spin density distribution (difference between charge densities for spin 'up' and 'down') obtained in LDA + U calculations for $KCuF_3$ [54]. Cu ions are in the corners of the cube, and F ions are in the middle of its edges. It can be seen that a single hole is localized on the $x^2 - y^2$ and $y^2 - z^2$ orbitals. This results in A-type antiferromagnetism shown by arrows.

this is completely due to corresponding orbital ordering, with the resulting highly anisotropic electron hopping and exchange interaction.

There are other materials in which orbital ordering leads to the formation of low-dimensional magnetic systems. A rather striking example is provided by pyrochlore $Tl_2Ru_2O_7$. In the latter, also crystallographically 3D cubic material with Ru^{4+} ($S = 1$) ions, a state with the spin gap appears below the phase transition at $T_c = 120$ K. However, structural studies have not revealed any apparent distortion which could have led to the formation of singlet dimers. The explanation proposed by Lee et al. [77] is that the orbital ordering appearing in $Tl_2Ru_2O_7$ below T_c leads to the formation of magnetically quasi-one-dimensional structures, viz. chains of $S = 1$ ions. Such objects — chains with integer spin — are very well known in 'spin science,' and they are called Haldane chains. In contrast to half-integer spin chains, they exhibit a gap (a spin gap) in the spin excitation spectrum [80, 81] and topologically protected edge (here ends of a chain) states.

4.2 '1D-zation' of electron spectrum and orbitally driven Peierls state

Other materials also exist with a similar reduction of effective dimensionality of the magnetic subsystem. But even more drastic consequences could result from the reduction of dimensionality in the electronic subsystem. This is often related to the special properties of low-dimensional, especially one-dimensional, systems and, in particular, to the tendency of such systems to undergo Peierls-like instability.

In Table 1, we list some materials in which the orbital structure leads to a reduction of the effective dimensionality of the electronic subsystem, in particular resulting in the formation of a Peierls-like state. Of course, we cannot describe in this review all these examples; we concentrate on the most representative (and easy to explain) cases.

Probably the most spectacular example concerns the formation of an exotic superstructure in $MgTi_2O_4$ (spirals) [74] and in $CuIr_2S_4$ (octamers) [72]. These materials belong

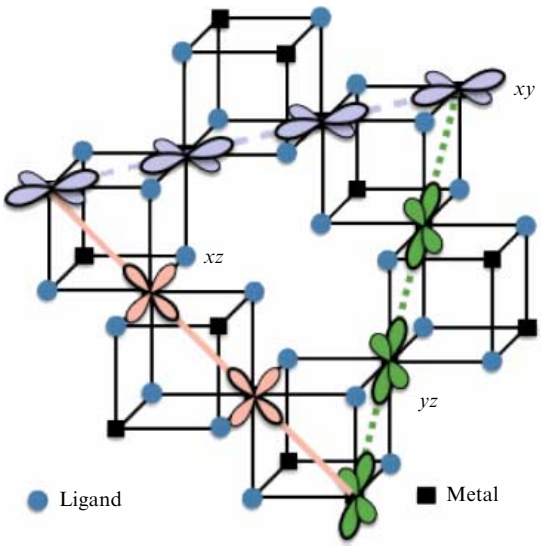

Figure 12. (Color online.) Formation of 1D chains in spinels due to orbital degrees of freedom. Transition metal ions (squares) reside at the B-sites of AB_2L_4 spinels. Ligands (L) are marked by blue dots.

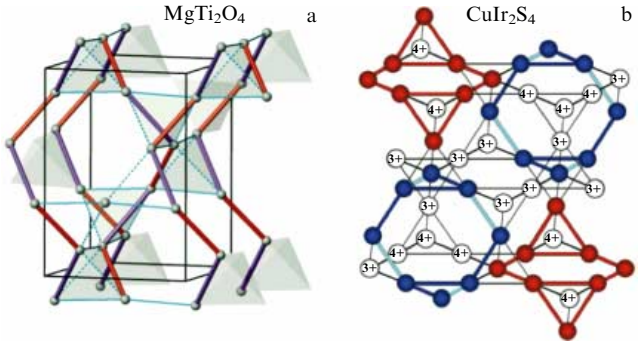

Figure 13. (Color online.) Crystal structures of $MgTi_2O_4$ and $CuIr_2S_4$ in the low-temperature distorted phase (taken from Refs [72, 74]). Transition metal ions are marked by circles. Short bonds in figure (a) are shown by violet lines, while long bonds by red lines. Red dots in figure (b) label Ir^{5+} ions, while blue dots label Ir^{4+} ions; chemical bonds in the Ir^{4+}–Ir^{4+} dimers are marked in light blue color.

to spinels with a TM ion in B-sites (Fig. 12). In both, a structural transition occurs from the cubic to tetragonal phases with decreasing temperature. But, besides that, in these systems extra distortions appear, leading to the formation of unusual superstructures. Thus, short (violet) and long (red) Ti–Ti bonds form strange 'spirals' in the low-temperature phase of $MgTi_2O_4$ (Fig. 13a).

An even more nontrivial superstructure was found by the same group in $CuIr_2S_4$ [72]: in this system at temperatures below 230 K there is a charge ordering of Ir ions (average valence $Ir^{3.5+}$) into $Ir^{4+}(t_{2g}^5)$ and nonmagnetic (low-spin) $Ir^{3+}(t_{2g}^6)$, and these species form beautiful octamers (Fig. 13b). Moreover, extra dimerization occurs in Ir^{4+} octamers with the formation of short Ir^{4+}–Ir^{4+} singlet dimers, which makes the whole material nonmagnetic.

In the original publications [72, 74], there was no explanation of the formation mechanism for these superstructures. But one can find a very straightforward explanation of the observed superstructures by taking into account the orbital dependence of the electronic structure in these spinels [73].

In both cases, we are dealing with systems comprising partially filled t_{2g} levels. As can be seen from Fig. 12, in spinels with TM ions at the B-sites, octahedra surrounding TM ions shore their edges. In this case a strong direct overlap of certain t_{2g} orbitals occurs in a particular direction. Thus, for example, the *xy*-orbital of one site strongly overlaps with a similar *xy*-orbital along the *xy*-direction, but not with the other two orbitals. Similarly, *yz*-orbitals overlap and experience strong hopping to the same *yz*-orbital in the *yz*-direction. Now, the structure of the B-sites of a spinel can be visualized as consisting of straight chains running in the *xy*-, *xz*-, and *yz*-directions. It may seem a rather artificial construction, but just for t_{2g} orbitals it acquires real significance. We see that electrons hopping from site to site — for example on the *xy*-orbital — would remain on the same orbital in the corresponding *xy*-chain, and similarly for the *xz*- and *yz*-orbitals. In effect, if we only include direct d–d overlapping and hopping, the electronic structure of these basically cubic materials would be composed of three one-dimensional bands: *xy*, *xz*, and *yz*.

Now, the famous Peierls effect tells us that the metallic state of such one-dimensional systems is unstable towards the formation of a superstructure which opens a gap at the Fermi

level (see Section 2). For half-filled bands, this would lead to dimerization — the well-known case. But actually, the same instability also develops for other band fillings. Thus, for quarter-filled bands, we would get tetramerization, for 1/3-filled bands trimerization, etc. And this was the explanation proposed in work [73] for superstructures observed in $MgTi_2O_4$ and $CuIr_2S_4$. One can easily see that in both these cases we would have 1/4-filled bands: doubly degenerate *xz*- and *yz*-bands in $MgTi_2O_4$, and 1/4- (rather more likely 3/4-) filled bands in $CuIr_2S_4$.

Thus, the exotic and puzzling superstructures observed in Refs [72, 74] find a natural explanation if one only takes the 'right viewing angle' and looks at what happens in 1D bands determining the electronic structure of these materials. In both these cases, we have a simple tetramerization on the straight chains: in the *xz*- and *yz*-chains in $MgTi_2O_4$, and in all directions in $CuIr_2S_4$. Thus, this rather highly simplified picture (we ignored, for example, possible electron hopping via ligands — oxygen, sulphur) gives a natural explanation of very exotic and beautiful superstructures found in $MgTi_2O_4$ and $CuIr_2S_4$ [73].

There are also other materials of the same kind in which this physics can be in action. For example, such can be the situation in V-based spinels, like ZnV_2O_4 [82, 83]. This material has caused quite a discussion in the theoretical physics community; several models have been proposed to explain the superstructure observed in it [84–88]. A final explanation of the properties of this system is still not agreed upon; but in any case, all proposed pictures were based on the important role of orbital degrees of freedom in determining its properties.

4.3 Novel states close to the Mott transition: 'molecules' in solids

In the previous sections, we have seen that in solids with correlated electrons some clusters, e.g., dimers, may appear in which electrons behave as practically delocalized, whereas still rather weak hopping takes place between such clusters. One can often describe such clusters using the treatment developed for molecules. In concentrated solids such objects can appear when the whole system is relatively close to a localized–itinerant crossover, i.e., close to the Mott transition.

Usually, when analyzing the Mott transitions, one thinks of the situation when on one side of the transition we have a homogeneous Mott insulator, and on the other side we are dealing with a homogeneous metallic state described, for example, by the Fermi-liquid theory. However, the experience collected in recent years has demonstrated that this is not the only possible situation. It turned out that in many real systems electron delocalization first occurred in finite clusters — dimers, trimers, or sometimes larger clusters — whereas weak hopping still took place between them, and the whole system still behaved as an insulator. And only at a later stage, e.g., at higher pressures, may the whole material become metallic.

Table 2. Metal–metal distances D_{met} in [Å].

3d	Ti 2.896	V 2.622	Cr 2.498	Mn 2.734	Fe 2.482	Co 2.506	Ni 2.492	Cu 2.556
4d	Zr 3.180	Nb 2.858	Mo 2.726	Tc –	Ru 2.650	Rh 2.690	Pd 2.752	Ag 2.890
5d	Hf 3.128	Ta 2.860	W 2.740	Re 2.742	Os 2.676	Ir 2.714	Pt 2.746	Au 2.884

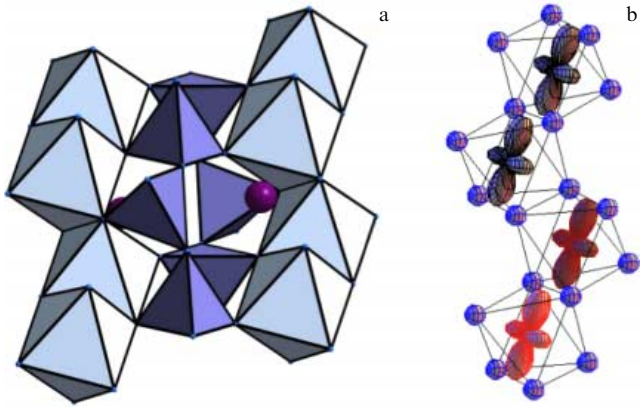

Figure 14. (a) Crystal structure of pyroxenes. Metal ions are inside octahedra which form zig-zag chains. (b) Orbital ordering, which is stabilized in the low-temperature phase of $NaTiSi_2O_6$.

In order to understand whether a system finds itself in such a state, one can compare the metal–metal distances in a compound under consideration with those met in pure metals, D_{met} (see Table 2). If some distances are smaller than D_{met}, then this can be a signature of the formation of 'molecules' in a given system.

The first example of the formation of such 'molecules' in bulk solids due to a particular orbital ordering is pyroxene $NaTiSi_2O_6$. Pyroxenes comprise a large class of materials which are not yet very popular among physicists, but which are extremely important in geology: they are silicates, one of the main rock-forming minerals. They constitute up to 30% of Earth's crust and are important constituents of the upper mantle [89]. They are quasi-one-dimensional compounds containing zigzag chains of MO_6 octahedra sharing common edges, and between them SiO_4 (or GeO_4) tetrahedra are located (Fig. 14a).

The material we want to discuss is $NaTiSi_2O_6$, with Ti^{3+} (d^1). It is paramagnetic, with susceptibility at high temperatures following a Bonner–Fisher curve for a one-dimensional antiferromagnet with $S = 1/2$. However, this behavior is interrupted at $T_c = 210$ K, below which it is practically diamagnetic [90].

Ab initio calculations demonstrate that, whereas at high temperatures one d-electron of Ti occupies more or less equally all three t_{2g} states, below T_c ferro-orbital ordering occurs, with filled orbitals depicted in Fig. 14b [35]. We see that after such ordering the system is practically divided into dimers, weakly connected with each other: the exchange coupling inside such dimers is strongly antiferromagnetic, $J \sim 400$ K, whereas the exchange between dimers is close to zero, and most probably is weakly ferromagnetic [35]. In effect, a material which was a one-dimensional antiferromagnet above T_c becomes split below T_c into singlet dimers. This is predominantly due to particular orbital ordering; one does not even have to move ions (but, of course, in reality the Ti–Ti distances inside and between these dimers also become different). This is a very clear example of reduced dimensionality and the formation of singlet 'molecules' due to the directional character of orbitals and due to a particular type of orbital ordering.

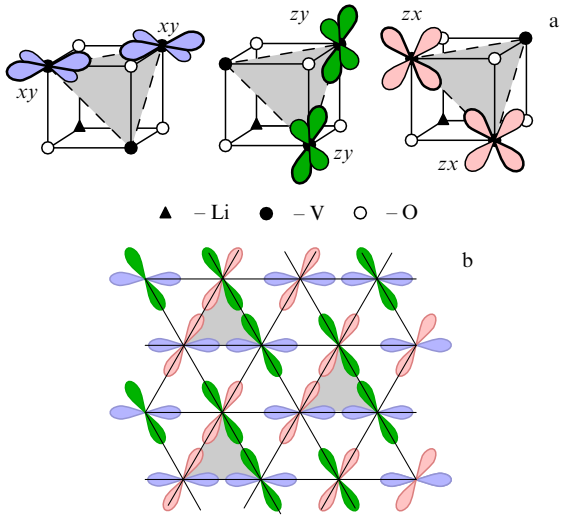

Figure 15. (Color online.) (a) Orientation of t_{2g} orbitals at B-sites of a spinel lattice, or $LiVO_2$, of Fig. 12. Out of three t_{2g} orbitals, there are two for each V site which have a direct overlap with neighboring V ions in $LiVO_2$. Two 'active' lobes (bold) of any of these orbitals responsible for this overlap lie in the triangular layer of V, while two other lobes are perpendicular to this plane. (b) Orbital ordering (only 'active' lobes are shown), which gives rise to trimerization in $LiVO_2$.

Another such example is $LiVO_2$. It can be visualized as a rocksalt VO in which half the V ions are substituted by nonmagnetic Li ions. V and Li ions in this case are ordered in consecutive [111] layers, and in effect we have a quasi-two-dimensional system, with V^{3+} (d^2) ions forming triangular layers separated by similar layers of nonmagnetic Li ions (see Fig. 15a).

$LiVO_2$ is an insulating compound, and at $T_c \sim 460$ K it experiences a structural phase transition, below which the magnetic susceptibility strongly decreases and $LiVO_2$ becomes practically diamagnetic, while it is paramagnetic above T_c [68]. This behavior was explained as being due to orbital ordering with concomitant structural distortion [91]. A triangular lattice is usually considered frustrated, meaning that it is not bipartite, i.e., it cannot be subdivided into two sublattices, such that the nearest neighbors of one belong to the other. But in $LiVO_2$, we have two d-electrons per one V ion, which occupy triply degenerate t_{2g} orbitals, so that from the 'orbital' point of view it is a triply degenerate system. These three t_{2g} orbitals are shown (by different colors) in Fig. 15.

And although triangular lattice cannot be subdivided into two sublattices, it can be naturally subdivided into three! This is what indeed happens in $LiVO_2$ below T_c. The orbital ordering proposed for $LiVO_2$ in Ref. [91] is demonstrated in Fig. 15b. We see that, due to this orbital ordering, the system is subdivided into tightly bound triangles (shaded in Fig. 15b). According to Goodenough–Kanamori–Anderson rules, one would have in these trimers a strong antiferromagnetic exchange (between the half-filled t_{2g} orbitals), whereas the exchange interaction between these trimers would be very weak and presumably ferromagnetic. In any case, antiferromagnetic coupling between V ions in these triangles, each V with $S = 1$ (two d-electrons per V), would make a spin-singlet ground state (three $S = 1$ spins form a total singlet (so to say, '$1 + 1 + 1 = 0$').

Indeed, representing the Heisenberg Hamiltonian for a triangle as

$$H = 2J(\mathbf{S}_1\mathbf{S}_2 + \mathbf{S}_1\mathbf{S}_3 + \mathbf{S}_2\mathbf{S}_3) = J(\mathbf{S}_1 + \mathbf{S}_2 + \mathbf{S}_3)^2 - J\sum_{i=1}^{3}\mathbf{S}_i^2 = J\mathbf{S}_{\rm tot}^2 - J\sum_{i=1}^{3}\mathbf{S}_i^2, \qquad (22)$$

we see that for the antiferromagnetic coupling ($J > 0$) the ground state corresponds to a total spin $S_{\rm tot} = 0$.

We would reach a similar conclusion if we treated d-electrons in these trimers as itinerant: in this case, these trimers would form just a triangular molecule with singlet dimers at each edge of a triangle, formed by respective orbitals (see Fig. 15b) with the $S_{\rm tot} = 0$ ground state. This picture would be more applicable if the effective d–d hopping within these trimers were larger than the Hund's rule coupling on each V, i.e., $t > J_H = 0.8-0.9$ eV. Which of these two limiting pictures is closer to reality in $LiVO_2$ is still an open question. Spectroscopic studies seem to be in favor of the first interpretation (localized electrons forming $S = 1$ spin at each V, which are coupled to total $S_{\rm tot} = 0$ in a trimer) [91]. However, structural distortion accompanying this transition in $LiVO_2$ leads to the formation of very short V–V bonds in such trimers: the V–V distance in these is 2.56 Å, even shorter than the V–V distance of 2.62 Å in a V metal [92]! From this point of view, one could expect that better description of V trimers can be obtained in a picture of electrons 'delocalized' within each trimer. Further studies, both experimental and theoretical, could be very helpful in resolving this dilemma.

Important information about the formation of clusters close to the Mott transition was provided by the experiments carried out by the Takagi group [69]. The authors extended the study of this phenomenon, observed in $LiVO_2$, to $LiVS_2$ and $LiVSe_2$ with the same structures, but with a stronger covalency than in oxide (Fig. 16). $LiVS_2$ undergoes a similar transition from the undistorted state to the diamagnetic one with the same trimers as in $LiVO_2$. But in this case, it is a real metal–insulator transition: $LiVS_2$ is a metal above T_c, but becomes an insulator in the trimerized phase below T_c. Going further to $LiVSe_2$, one reaches a real metallic state which survives down to $T = 0$. Thus, we have spanned in these systems the whole series of phase transitions: an insulator–

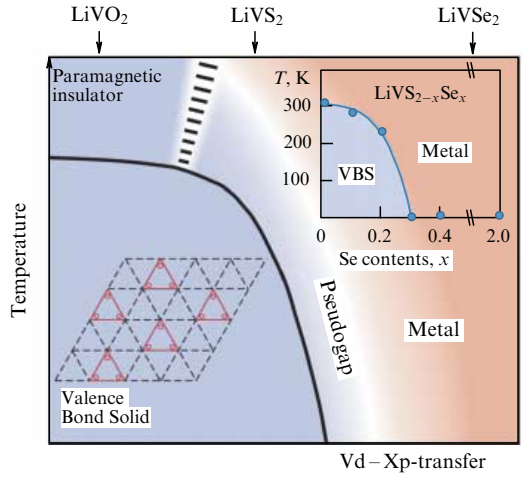

Figure 16. (Color online.) Schematic phase diagram of $LiVL_3$, where L is O, S, or Se. (Taken from Ref. [69].)

insulator transition in $LiVO_2$, a metal–insulator transition in $LiVS_2$, and a homogeneous metallic state in $LiVSe_2$. Apparently, the formation of these tightly bound trimers in $LiVO_2$ and $LiVS_2$ is intrinsically connected with the proximity to such a localized–itinerant crossover, or to a Mott transition, and can be seen as a precursor of this transition.

The example of $LiVO_2$ also clearly indicates that the 'molecules' formed close to the Mott transition can be not only dimers, which we encounter, e.g., in VO_2 [2] or $NaTiSi_2O_6$ [90], but also larger clusters — in this case, V_3 trimers. There are also examples of still larger molecular clusters formed in this situation. For example, tetramers are formed in CaV_4O_9 [93]. One can also speak about tetramer molecules in so-called lacunar spinels like GaV_4O_8, which can be visualized as distorted A-site deficient spinels $Ga_{1/2}(\text{vacancy})_{1/2}V_2O_4$. In this case, one can very successfully describe their electronic structure by molecular orbitals in respective clusters, and such 'molecules' can even form Mott insulators, with these clusters playing the role of sites in the Mott–Hubbard description of these systems [94, 95]. Actually, a very similar situation also exists in pure and doped C_{60} buckyballs, for example, in K_3C_{60}, where electrons 'live' on the molecular orbitals of C_{60} balls and, depending on the occupation of respective molecular levels, we may have either singlet ('low-spin') states or states with magnetic moments localized on such molecules [96]. Under certain conditions, we can observe here insulator–metal transitions, and in the metallic state the materials can even become superconducting [97].

There also are other systems with similar properties. Even larger molecular clusters are formed in the spinel AlV_2O_4, where below the metal–insulator transition a structural deformation occurs with the formation of V heptamers — clusters comprising seven V ions (see Fig. 17) [70]. And, similar to $LiVO_2$, at least some V–V bonds in these 'molecules' are shorter than those in a V metal.

One can sometimes also apply this concept of 'molecules' in solids to systems in which there are no such clusters structurally. Even in this case, there can be situations in which, electronically, one can describe a system as composed of 'molecules'.

The honeycomb geometry is very interesting from this point of view. Let us consider TM ions in the octahedral coordination with a not completely filled t_{2g} shell. These

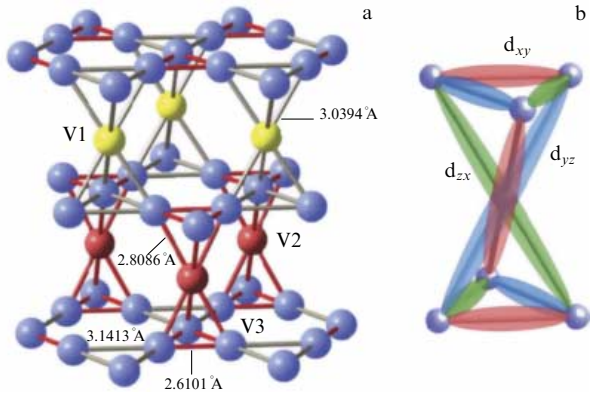

Figure 17. (Color online.) (a) Crystal structure of AlV_2O_4 (only V ions are shown). Vanadium heptamers formed by short V–V bonds are marked in red. (b) Suggested molecular orbitals, which result in the formation of these heptamers. Reproduced from Ref. [70].

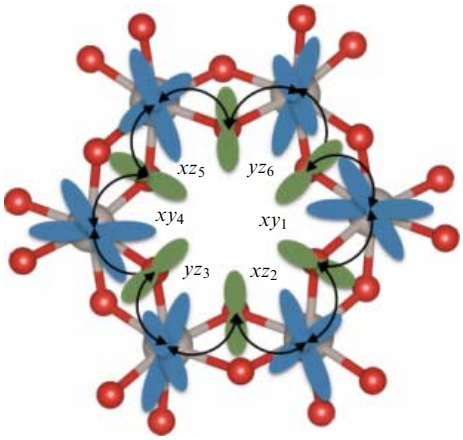

Figure 18. (Color online.) Formation of quasimolecular orbitals on a honeycomb lattice via p–d hopping in $SrRu_2O_6$. Transition metal ions are shown in grey, ligands by red balls. Starting from one of the t_{2g} orbitals (blue), the d-electron turns out to be confined in the quasimolecular orbital on one of the hexagons, if only the hopping via p-orbitals (green) of the ligands are taken into account.

octahedra form a honeycomb lattice sharing their edges, as, e.g., in Na_2IrO_3 or $SrRu_2O_6$. If one includes hoppings via ligand p-orbitals, then, due to the signs of the wave functions in such a geometry, the d-electron can hop only within one particular hexagon and cannot move to another one, as shown in Fig. 18. Thus if we start, for instance, from the xy_1-orbital on a site *1*, then the electron can hop only to the xz_2- and yz_6-orbitals of neighboring TM ions in a certain hexagon (subscripts numerate TM ions). Being on these orbitals, it cannot escape this TM_6 hexagon, but can only move to the yz_3- and xz_5-orbitals, and so on. Thus, the nature of electrons in this case is twofold [98]. On the one hand, they are itinerant within the hexagon, but, on the other hand, localized on some extended orbitals, which are called quasimolecular orbitals (QMOs) [99]. It is interesting that QMOs give rise to a band spectrum reminiscent of the electronic spectrum of a benzene molecule.

This type of description of the electronic structure in TM oxides having a honeycomb lattice was first proposed for Na_2IrO_3 and Li_2IrO_3 [99, 100]. However, it turned out that in iridates this model is still not perfect; there are effects which lead to 'mixing' of these QMOs, such as direct d–d hopping and the SOC (see Section 6.5 for details). But, for example, in $SrRu_2O_6$, this picture works much better [98]. In $SrRu_2O_6$, the presence of these QMOs is expected to strongly affect the optical properties [101] and could also be important for describing its unusual magnetic properties, in particular, a Néel temperature of $T_N \sim 560$ K, very high for the layered material [102, 103].

It is clear that direct d–d and p–d hoppings on a honeycomb lattice would stabilize very different states. The p–d hoppings via the ligand p-orbitals may result in the formation of QMOs living on hexagons (Fig. 18), while the direct d–d hopping would favor a strong metal–metal bond on particular two-site bonds (Fig. 19). It can be seen that in this case an electron, put on such a t_{2g} orbital, can only hop to one nearest neighbor TM ion and back. Thus, the effective dimensionality in this case would be reduced from 2D to 0D! This serves as a clear example of reducing the effective dimensionality due to orbital ordering, discussed in Section 4.1. Indeed, there is one t_{2g} orbital at each site in the

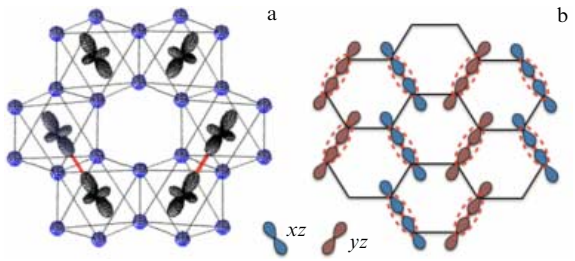

Figure 19. (a) Orbitals providing strong direct d–d bonding and finally leading to the formation of the spin-singlet state in Li_2RuO_3 (the results of GGA calculations). (b) Herringbone distribution of these singlets, found in the low-temperature phase of Li_2RuO_3 [105, 106].

common edge geometry, directed towards a neighbor, which would give such a strong bonding (cf. Fig. 6b).

The relative importance of the d–d or p–d hoppings depends on the particular situation. In the case of a large metal–metal distance, the dominant hopping would occur via ligands (since t_{dd} falls drastically with distance, as may be inferred from Eqn (11)); but for short distances, direct d–d hopping may dominate. It seems that, for example, Na_2IrO_3 belongs to the first class of systems, whereas Li_2IrO_3, with smaller Li ions, may already be 'half-way' to the second case with dominating d–d hoppings. This, in particular, may be responsible for a more complicated magnetic structure of Li_2IrO_3 compared with Na_2IrO_3 [104]. Distortions of the octahedra surrounding TM ions and the SOC can also intervene.

Speaking of honeycomb systems, it is interesting to compare the situation in '213' iridates like Na_2IrO_3 and Li_2IrO_3 with that in Na_2RuO_3, i.e. in a similar system with Ru instead of Ir: Li_2RuO_3. The latter may be an example of a system of the second type, in which the direct d–d hopping may be more important than that via oxygen. Although Na_2IrO_3 and Li_2IrO_3 remain undistorted and at low temperatures they exhibit long-range magnetic ordering [104], a phase transition in Li_2RuO_3 occurs below $T_c \sim 540$ K with the formation of diamagnetic dimers from Ru ions [105, 106], with the Ru–Ru distance in the dimer being rather short, 2.57 Å [105] — again, shorter than that in a Ru metal (2.65 Å). Below T_c, these dimers form an interesting herringbone pattern. The formation of such dimers, as explained in Ref. [107], is a consequence of an orbital ordering, with the direct d–d hopping playing the main role (Fig. 19). *Ab initio* calculations support this picture in general, although it seems likely that the hopping via oxygens is not negligible either. Interestingly enough, the dimer Ru–Ru 'molecules,' ordered in Li_2RuO_3 below 540 K, are very stable, and they persist even above T_c in the 'averaged' hexagonal phase. A pair distribution function (PDF) study has demonstrated that they survive locally up to at least 650 °C, forming a disordered and probably dynamic (liquid-like) state — a dimer liquid [108]. NMR data also detect thermal activation processes associated with the flow of dimers [109]. The study of this system for different stoichiometry supports such a conclusion [110].

In which cases in such honeycomb systems one ends up with an undistorted lattice (a long-range magnetic order will appear at low temperatures) and when it is more favorable to form singlet dimers ordered in a particular fashion is an interesting and still an open question. As we just argued, one can present qualitative arguments that, when the direct d–d hopping dominates, there may be better conditions for the formation of a 'molecular' state (another name for such a state is a valence bond solid [111]). The dominant hopping via oxygen p-orbitals of ligands may work rather in favor of less localized states, although the notion of molecular, or more precisely quasimolecular, orbitals may be applicable in such cases, too.

In any case, all these examples demonstrate that novel states may indeed appear close to a localized–itinerant crossover, so that the Mott transition occurs 'stepwise': first, the electrons are delocalized in finite clusters, forming 'molecules' in a solid — the hopping between such molecules being still small enough to render the whole system insulating, but with electrons localized rather on such 'molecular clusters' and not on isolated sites. Only later, for example, at still much higher pressures, can one reach a state of a homogeneous metal in which electrons would really be itinerant, delocalized over the whole system. This is, of course, not a universal behavior — for example, it strongly depends on the lattice geometry (being less plausible for systems like perovskites with corner-sharing MO_6 octahedra); but in many cases, one should indeed expect — and actually observe — such a behavior.

5. Orbital-selective effects

5.1 Orbital-selective Mott transition

Generally speaking, a separation of all electrons into those exhibiting itinerant behavior and those, which are more localized, can occur not only in real space due to the formation of finite size clusters, but equally well a system may stay uniform even on a small scale but have electrons of a very different character: 'insulating' and 'metallic.' In other words, the Mott transition may not occur simultaneously for all bands, but in turns, i.e., it can be orbital-selective. The term 'orbital-selective Mott (OSM) transition' was coined by Anisimov et al. [113] to describe the electronic properties of $Ca_{2-x}Sr_xRuO_4$, when it was found that the transition to an insulating state for the narrow xz/yz-bands occurs at much smaller values of U than for the xy-band with a larger bandwidth. Thus, in the regime of large U, the whole system is insulating due to correlation effects, while for small U it is metallic; but in the intermediate regime some of the electrons are localized, while others are itinerant.

Since there are two very different kinds of electrons, one needs to apply the Hubbard model with inequivalent orbitals (bands) to describe such a situation. The simplest would be the two-band Hubbard model with different nearest neighbor hoppings t_m:

$$H = -\sum_{\langle ij\rangle m\sigma} t_m c^{\dagger}_{im\sigma} c_{jm\sigma} + U\sum_{im} n_{im\uparrow} n_{im\downarrow} + U'\sum_{\substack{i\\ m\neq m'\sigma\sigma'}} n_{im\sigma}\, n_{im'\sigma'} - J_{\rm H}\sum_{i\sigma\sigma' mm'} c^{\dagger}_{im\sigma} c_{im\sigma'} c^{\dagger}_{im'\sigma'} c_{im'\sigma}\,, \quad (23)$$

where i, j and m, m' are the site and orbital indexes, respectively, U and $U' = U - 2J_{\rm H}$ are intra- and interorbital interactions, and $J_{\rm H}$ is Hund's rule exchange interaction (one could also consider different on-site energies of these two d-levels, e.g., due to the crystal-field effects; see below); in the 3rd and 4th terms, summation runs over each pair of m, m'. The phase diagram of such a model in the case of $J_{\rm H} = 0$ and half-filling of sites (i.e., for two electrons per site) on a 2D

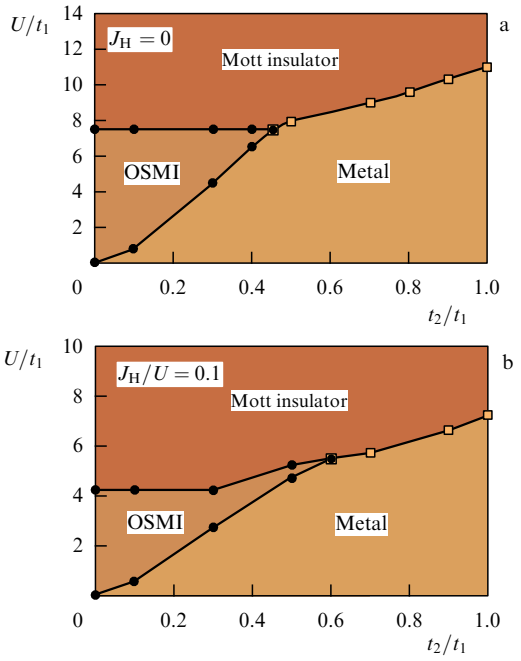

Figure 20. Phase diagram of the two-band nondegenerate Hubbard model on a square lattice, illustrating the onset of the orbital-selective Mott insulating (OSMI) phase: (a) $J_H = 0$, while (b) $J_H/U = 0.1$. (Reproduced from Ref. [112].)

square lattice is shown in Fig. 20a [112]. There are three main regions: (1) a homogeneous metallic state, when $t_2/t_1 \to 1$ and U is small; (2) an insulating Mott phase at large U, and (3) an intermediate OSM phase (we ignore here possible complications like the eventual formation of the spin-density wave (SDW) state due to the nesting of the Fermi surface, which could appear even at small U).

It is important to mention that the phase diagram presented in Fig. 20 was obtained for an ideal situation, when there is no mixing among different orbitals in the kinetic energy term. Any hybridization between these orbitals, i.e., the presence of terms like $t_{mm',ij}c^{\dagger}_{im\sigma}c_{jm\sigma}$ with $m \neq m'$, would suppress the OSM state. Such terms are always present in real systems and they disfavor the OSM phase. However, there are also other factors which, in contrast, stabilize such a state. First of all, the Hund's rule intraatomic exchange interaction J_H suppresses any orbital fluctuations irrespective of U and thus supports the OSM state, as one can easily see comparing the top and bottom panels in Fig. 20. There are also other factors, which help to decouple different orbitals. For example, it was shown in Ref. [114] that the OSM phase may appear even in the situation when two bands have the same bandwidths (i.e., $t_1 = t_2$), but there is crystal-field splitting supported by the Hund's exchange.

In the same way as the formation of 'molecules' in homogeneous solids (described in Section 4.3), the OSM phase is a precursor of a phase transition. It should be noted that the OSM phase is not simply a theoretical toy, but that the orbital selectivity strongly affects the physical properties of the systems of interest. For example, the orbital-selective localization leads to a non-Fermi-liquid behavior [115]. Moreover, it is well known that an insulating state can be obtained only for integer site occupancies in the Hubbard model, and any doping makes a system metallic. In contrast, the OSM phase is robust against doping [116]. This can be easily rationalized, since doping changes only the position of the chemical potential μ within the metallic band formed by itinerant electrons, and the OSM phase is stable until the total change in μ exceeds the energy gap provided by localized electrons.

The influence of the electron–phonon interaction on the OSM state has very recently been studied in the framework of the Hubbard–Holstein model with two electronic bands having very different bandwidths ($t_1/t_2 = 5$) [117]. In particular, it was found that if we change the strength λ of the electron–phonon interaction, then the transition from the uniform metallic state to the phase with the charge-density wave (CDW) also occurs through the orbital-selective phase (with a site-centered CDW).

It has to be mentioned that the idea of the OSM state was implicitly used long before paper [113]. Indeed, for example, in order to explain the double exchange mechanism of ferromagnetism, one needs to treat some electrons as itinerant, moving against the background of localized magnetic moments provided by completely different electrons, which essentially do not hop from site to site (see Section 3.3). This is actually the picture always used to describe, for example, the properties of the colossal magnetoresistance in manganites $La_{1-x}Sr_xMnO_3$ and $La_{1-x}Ca_xMnO_3$ [41]. For these systems, one usually treats electrons in the half-filled t_{2g} shell (t^3_{2g}) as localized, and the electrons in the e_g bands as itinerant. This picture was already described in Section 3.3. We could, in principle, also include correlation effects for the e_g electrons, but even without those, the purely itinerant picture of the e_g electrons gives a very reasonable description of many properties of these manganites [118]. The same description (t_{2g} electrons localized, e_g itinerant) can also be successfully used for other systems with perovskite and perovskite-related structures. Ideas similar to the OSM state were previously used in the Kondo physics, e.g., for the description of the heavy-fermion compounds, for which the electrons from different shells are usually considered localized (typically f-electrons) or mobile (s, p, d).

5.2 Orbital-selective behavior and (partial) suppression of magnetism

We have already seen that the formation of molecular orbitals, promoted by corresponding orbital occupation, can weaken and even completely suppress magnetism in some materials, e.g., in $NaTiSi_2O_6$, $CuIr_2S_4$, and $LiVO_2$ (see Sections 4.2, 4.3).

But we can also anticipate a situation in which the electrons on one orbital form a singlet state, whereas other electrons still remain localized and contribute to magnetism — albeit with a significantly reduced moment. Or these electrons can be regarded as delocalized, but not forming singlet dimers. Such a situation would be in some sense analogous to the orbital-selective behavior described in the previous subsection. It can be illustrated with a simple model, which, as we show below, actually rather closely corresponds to the experimental situation observed in some real materials.

Consider a dimer with two orbitals on each site, with strong intersite hopping t_c from one orbital, call it c-orbital, and no (or very small) hopping t_d from the other d-orbital:

$$H = -\sum_{\langle ij\rangle\sigma}(t_c c^{\dagger}_{i\sigma}c_{j\sigma} + t_d d^{\dagger}_{i\sigma}d_{j\sigma}) - J_H\sum_i\left(\frac{1}{2} + 2S^z_{id}S^z_{ic}\right),$$

and consider the case of two electrons per site. If the Hund's coupling J_H is the largest parameter in the system, first both

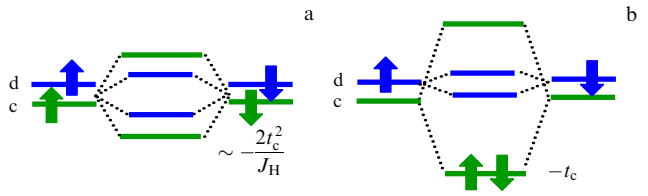

Figure 21. Scheme of energy levels illustrating the formation of an orbital-selective state. In the left panel (a), the conventional state with spin $S = 1$ per site (due to the dominating Hund's intraatomic exchange) is presented. In the right panel (b), the orbital-selective state is formed in the case of two orbitals and two electrons per site.

electrons at each site form, according to the first Hund's rule, the state with spin $S = 1$ (Fig. 21a). These electrons would then have some exchange because of virtual hopping of c-electrons between sites, which would give an antiferromagnetic coupling of these spin $S = 1$ sites with the exchange constant $J \sim 2t_c^2/J_H$ (cf. the usual expression (9) for the exchange interaction in the simple Hubbard model; here, we have not yet included the Hubbard repulsion U, but the virtual state with an electron transferred to a neighboring site has an excitation energy J_H, which now stands in the denominator of the expression for J instead of Hubbard's U in formula (9)). If $t_d = 0$, the energy of this state is given by

$$E_{LS} = -2J_H - \frac{2t_c^2}{J_H}\,. \tag{24}$$

However, for small J_H and large enough hopping t_c, we can find a very different state (Fig. 21b): it is possible to make a singlet from the c-electrons, breaking the $S = 1$ states at each site, stabilized by the Hund's exchange interaction. Then we lose (a large part) of the Hund's energy. But instead of that, these c-electrons can now gain bonding energy $-2t_c$. The energy of such a state would be

$$E_{OS} = -2t_c - J_H \tag{25}$$

for $t_d = 0$ (part of the Hund's energy we still gain when c- and d-electrons are at the same site with their spins aligned parallel). In any case, a comparison of these expressions (24) and (25) shows that this second state, with two electrons occupying molecular orbitals formed by the c-orbitals, is more favorable if the inequality

$$t_c > \frac{J_H}{2} \tag{26}$$

is satisfied. In this state, the remaining d-electrons, one per site, would live their 'own life' irrespective of the c-electrons; for example, they can experience magnetic ordering, but with a strongly (here twofold) reduced magnetic moment: spin 1/2 per site instead of spin 1 for a dominating Hund's coupling. Therefore, this state can be called orbital-selective [119].

We have mentioned that the idea of orbital selectivity lies at the heart of the double exchange, but how may this differentiation on the c- and d-orbitals occur? In fact, this is a very natural situation in many geometries. For example, the xy-orbitals will have much larger direct hoppings than xz- or yz-orbitals in a 'common edge' geometry (Fig. 6b), or the a_{1g} orbitals overlap much more strongly than e_g^π in a common face case (Fig. 6c). This is the reason why orbital selectivity is not such a rare phenomenon.

Let us consider, for example, α-$MoCl_4$, where Mo^{4+} ions have the $4d^2$ configuration. One might expect that the effective Curie–Weiss magnetic moment in this situation would be $\mu_{eff} \sim 2.8\mu_B$, but in fact it turns out to be much smaller: $\mu_{eff} \sim 0.9\mu_B$ [120, 121]. This is because of the large overlap between the xy-orbitals (c-orbitals), which is caused by singlet molecular orbitals, so that the magnetic moment is provided only by the electrons occupying the xz/yz-orbitals (d-orbitals) [122].

Another example of such a behavior is provided by rutile type systems VO_2 and MoO_2. In VO_2 (V^{4+}, d^1), the famous metal–insulator transition at 68 °C is accompanied (or is driven by) the formation of V–V dimers in chains in the c-direction, where VO_6 octahedra share a common edge, the dimers being formed by corresponding xy-orbitals (in a local coordination system). In contrast, MoO_2 (Mo^{4+}, d^2) remains metallic down to $T = 0$. Nevertheless, the structure of dimers formed in MoO_2 from TM ions entirely coincides with that of V–V dimers formed in VO_2 at temperatures below T_c! Apparently, the electrons on the xy-orbitals in MoO_2 form such singlet dimers, whereas the other electron per Mo behaves quite differently, in this case forming a metallic band. This is also a very clear example of orbital-selective behavior.

It is important to note that the orbital-selective behavior can be seen not only in the case of the integer number of electrons per site, but also for other fillings. For example, in the case of an isolated dimer with 3 electrons (1.5 electrons per site), one can easily find the energies of the two energetically lowest solutions. The first one, shown in the inset (a) to Fig. 22, is a 'molecular' version of the DE: the c-electron hops from site to site and forces d-electrons to have the same spin projection (we chose $t_d = 0$ for simplicity); the energy of this state is

$$E_{DE} = -J_H - t_c\,. \tag{27}$$

This state has the maximum total spin $S_{tot} = 3/2$ (it corresponds to the ferromagnetic order in the conventional DE).

However, there is also another state, that with $S_{tot} = 1/2$, sketched in the lower part of Fig. 22. In this state, two electrons occupy the bonding state constructed out of the c-orbitals. This state is stabilized by a large hopping t_c between c-orbitals. It is an orbital-selective (OS) state in the sense that only part of the d-electrons provide the spin

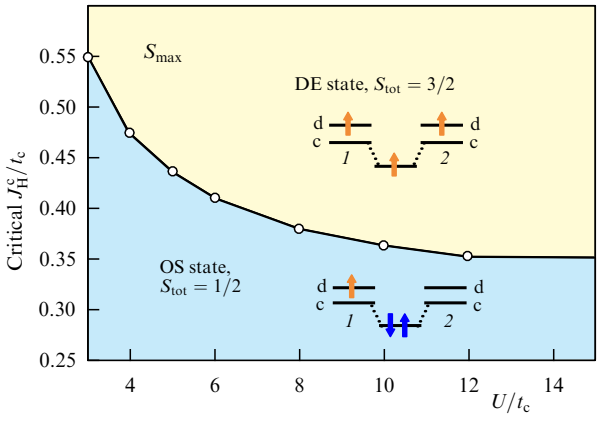

Figure 22. Phase diagram for a dimer with 2 orbitals and 1.5 electrons per site in U (on-site Hubbard repulsion) and J_H (Hund's rule exchange coupling) coordinates. Results of the exact diagonalization at $T = 0$ [52].

moment, while electrons on other (c) orbitals form a singlet spin state. The energy of this state is given by

$$E_{\rm OS} = -\frac{J_{\rm H}}{2} - 2t_{\rm c}\,. \tag{28}$$

We see that these two states will compete, and the total spin of the system can be suppressed if

$$2t_{\rm c} > J_{\rm H} \tag{29}$$

[cf. formula (26)]. While in the double exchange-like treatments, $J_{\rm H}$ is typically treated as the leading parameter, and the condition (29) of OS–DE competition can be considered unrealistic, in real materials it can be easily fulfilled. As was already mentioned above, this may be the case observed in some 4d and 5d systems, for which the Hund's coupling is weaker, but the larger extension of d-functions results in increasing the value of intersite hopping t.

One such example is provided by the $Y_5Mo_2O_{12}$ compound, which has the structure of dimerized chains [123], and in which the Mo ion has the $4d^{1.5}$ electronic configuration — the same as considered above. The dimers are formed by the edge-sharing MoO_6 octahedra (see inset to Fig. 23). There is a very strong overlap between the xy-orbitals in this geometry. Corresponding bonding–antibonding splitting exceeds 2.9 eV, and $t_{xy/xy} \sim 1.4$ eV, while $t_{xz,yz/xz,yz} \sim 0.3$ eV [88]. Thus, we see that $2t_{\rm c} \approx 2.8$ eV is much larger than any possible values of the Hund's coupling $J_{\rm H}$ (typically $\sim 0.5-0.7$ eV for the 4d elements). Thus, in this case, as in our toy model, the xy-orbitals form a singlet state on a dimer, which results in a considerable reduction in the magnetic moment observed in this system: $\mu_{\rm eff}^{\rm exp} = 1.7\mu_{\rm B}$/Mo [123], which is much smaller than $\mu_{\rm eff}^{\rm theor} = 2.3\mu_{\rm B}$/Mo expected for $Mo^{4.5+}$.

A situation very similar to that in $Y_5Mo_2O_{12}$ is also observed in $Y_5Re_2O_{12}$ possessing the same crystal structure [124]. In this system, with the Re ion valence 4.5+ (electronic configurations d^2/d^3), the magnetic moment per dimer is again strongly suppressed, even more significantly than in $Y_5Mo_2O_{12}$: it corresponds to $S = 1/2$ per dimer, instead of the spin 5/2 expected if the 'DE' state were realized. In this way, here *two electrons* per Re ion form singlet metal–metal bonds, and only one electron per dimer remains magnetic.

The treatment of the orbital-selective formation of 'molecules,' which was presented above, is rather qualitative, since it does not take into account the strong on-site Hubbard repulsion which is typical of TM ions. But one can easily generalize it by an exact treatment of a dimer case. The results of the exact diagonalization for an isolated dimer, described by the Hamiltonian

$$H = -\sum_{\langle ij\rangle\,\sigma}(t_{\rm c}c^{\dagger}_{i\sigma}c_{j\sigma} + t_{\rm d}d^{\dagger}_{i\sigma}d_{j\sigma}) + U\sum_{im} n_{im\uparrow}n_{im\downarrow}$$
$$+ U'\sum_{im\neq m'} n_{im\uparrow}n_{im'\downarrow} + \frac{U'-J_{\rm H}}{2}\sum_{\substack{i\sigma\\ m\neq m'}} n_{im\sigma}\,n_{im'\sigma'}\,,$$

in which we also included this interaction, are presented in Fig. 22. They clearly show that the critical ratio $J_{\rm H}/t$ for the suppression of the DE solution depends on Hubbard U (in the so-called Kanamori parameterization $U' = U - 2J_{\rm H}$ [31]).

As we have seen for the example of $Y_5Mo_2O_{12}$, the suppression of the magnetic moments due to orbital selectivity not only occurs in isolated clusters, but it was shown to persist in dimerized systems, which can be considered an intermediate step between isolated clusters and uniform solids. One might expect that this mechanism will play an important role in solids as well, but certainly in them it will be much less pronounced. Beside that, while in a dimer there is a discontinuous transition from the DE to the OS state (since they correspond to different quantum numbers), it becomes a smooth crossover in dimerized bulk systems, and the final value of the measured magnetization depends on specific parameters of the system under consideration (see Fig. 24).

In this connection it is very interesting to mention systems with the general formula $Ba_3MRu_2O_9$, where M can be In, Y, La, Lu, Nd, etc. (in principle, one can also have at these positions the other ions like Na^{1+}; Ca^{2+}, Co^{2+}; Ce^{4+}, Ti^{4+}). Ru ions are in the RuO_6 octahedra, which form dimers ordered in the triangular lattice. Since Ru ion valency is 4.5+, one may expect that the local magnetic moment on a Ru ion would be $\sim 2.5\mu_{\rm B}$. However, while the crystal structures of systems with different M-ions are almost the same [125, 126], their magnetic properties differ widely [127, 128], and none of them resembles a system with the local magnetic moment equal to $\sim 2.5\mu_{\rm B}$. For instance, in

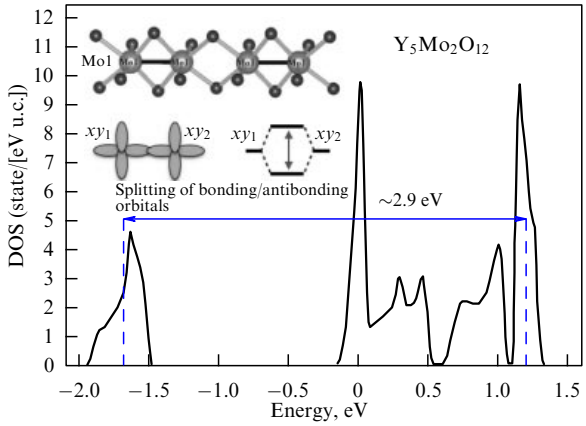

Figure 23. Density of electronic states pr unit cell as obtained in *ab initio* calculations in the generalized gradient approximation for $Y_2Mo_5O_{12}$ [88]. Crystal structure and 4d orbitals of Mo, which greatly overlap, are shown in the insets.

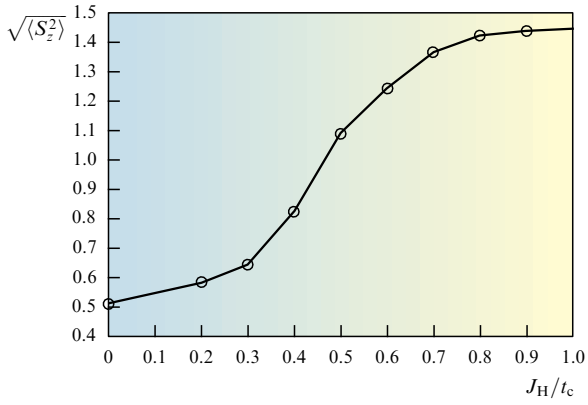

Figure 24. Results of cluster DMFT calculations for a dimerized chain with 2 orbitals and 1.5 electrons per site (for details, see paper [52]). It can be seen that there is a wide crossover region, where the total spin per dimer can have any value between $S_{\rm tot} = 1/2$, corresponding to the OS state, and $S_{\rm tot} = 3/2$ of the DE solution.

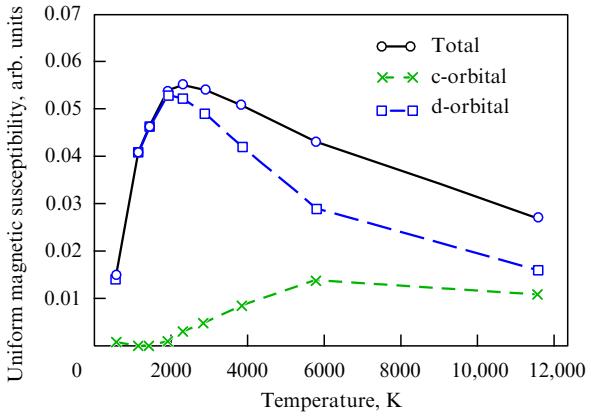

Figure 25. Magnetic susceptibility as obtained in cluster DMFT calculations for a dimerized chain with two orbitals (c and d, $t_c \gg t_d$) and two electrons per site (for details, see paper [130]).

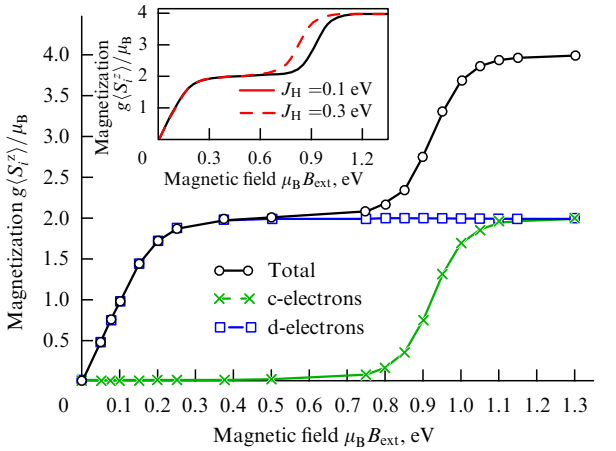

Figure 26. Results of cluster DMFT calculations for a chain consisting of dimers. Magnetization dependence on applied field in the orbital-selective regime. It can be seen that, first, the localized d-electrons respond to the applied magnetic field, and only later the molecular-like c-electrons join them (for details, see paper [130]).

$Ba_3YRu_2O_9$, the local magnetic moment on Ru is $\sim 0.5\mu_B$, while in $Ba_3LaRu_2O_9$ it is $\sim 1.4\mu_B$ [126]. Different models, like charge ordering (i.e., segregation on Ru^{4+} and Ru^{5+} ions) [128] and double exchange [126], have been involved to explain the magnetic properties of the $Ba_3LaRu_2O_9$ series. In fact, they can be explained considering orbital-selective behavior of compounds with the crystal structure playing the role of a fine tuner which regulates splittings between different molecular or localized orbitals and, because of this, influences the magnitude of the magnetic moment observed [129].

One may expect many different manifestations of the orbital selectivity. For example, since there are two types of orbitals, namely c-orbitals having a tendency to form molecular orbitals, and the d-orbitals whereon the electrons, on the contrary, behave more like localized ones, these electrons can react very differently to external perturbations.

In Fig. 25, the temperature dependence of the magnetic susceptibility obtained in the cluster DMFT calculations for a dimerized chain with two orbitals (c and d, again $t_c \gg t_d$) and two electrons per site is presented. It can be seen that the low-temperature response (which, in particular, determines the value of the spin gap in excitation spectrum) is due to localized (d) electrons only, molecular-like c-electrons being in a singlet state, so that they enter the game at a much higher temperature. Such behavior may also give the plateau in the external magnetic field dependence of the magnetization, as one may see from Fig. 26 [130].

The situation in real materials is, however, more complicated. Thus, one might expect the orbital-selective behavior in Li_2RuO_3, which was already discussed in Section 4.3. Because of the common edge geometry, there are strongly overlapping *xy*-orbitals (Fig. 6b), which play the role of c-orbitals, the *xz*-, *yz*-orbitals playing the role of localized d-orbitals, such that $t_{xy/xy} \gg \{t_{yz,yz}, t_{xz,xz}\}$. However, the LDA + DMFT calculation for these materials shows only a moderate difference between contributions from different orbitals to the magnetic susceptibility [109]. This is a result of a sufficiently low symmetry (substantial distortions of the crystal structure), which leads to an orbital mixing and to a partial 'magnetization' of the *xy*-orbitals.

Although investigating such subtle effects as different orbital contributions to the total magnetic susceptibility requires further theoretical and experimental studies, a general concept of orbital selectivity works very well in many dimerized systems. In Table 3, one may find a number of examples for which it is seen that the theoretical magnetic moments expected from the ionic configuration of a transition metal ion are much larger than the experimental values. An agreement between theory and experiment might only be achieved taking into account the orbital-selective formation of molecular orbitals, which substantially reduces theoretical magnetic moments.

One may notice that most of the TM ions in Table 3 are 4d and 5d TM ions, not 3d. The main reason for this was already discussed above: a much larger spatial extension of the 4d and 5d wave functions as compared to 3d ones [due to a larger

Table 3. Examples of dimerized systems, in which the orbital-selective formation of molecular orbitals results in a considerable reduction in magnetic moments compared to what one would expect on the basis of an ionic configuration of a transition metal ion.

System	Ionic configuration	Local (μ) or effective (μ_{eff}) moment	
		Theoretical	Experimental
$Y_5Mo_2O_{12}$	$4d^{1.5}$	$\mu_{eff} = 2.3\mu_B$/Mo	$\mu_{eff} = 1.7\mu_B$/Mo [123]
$Nb_2O_2F_3$	$4d^{1.5}$	$\mu_{eff} = 3.9\mu_B$/dimer	$\mu_{eff} \approx 2\mu_B$/dimer [131]
α-$MoCl_4$	$4d^2$	$\mu_{eff} = 2.8\mu_B$/Mo	$\mu_{eff} \approx 0.9\mu_B$/Mo [121]
$Ba_3YRu_2O_9$	$4d^{3.5}$	$\mu = 2.5\mu_B$/Ru	$\mu = 0.5\mu_B$/Ru [126]
$Ba_3LaRu_2O_9$	$4d^{3.5}$	$\mu = 2.5\mu_B$/Ru	$\mu = 1.4\mu_B$/Ru [126]
$Ba_5AlIr_2O_{11}$	$4d^{4.5}$	$\mu_{eff} = 3.3\mu_B$/dimer	$\mu_{eff} \approx 1\mu_B$/dimer [132, 133]

principal quantum number (see, e.g., Ref. [3])]. On the one hand, this results in an increase in the hopping parameters and, on the other hand, it leads to a decrease in the Hund's exchange. Intradimer hoppings for the 4d and 5d systems may be quite large, and the resulting bonding–antibonding splitting may exceed 3 eV [88]. On the other hand, while typical J_H for 3d TM are ~ 1 eV, they are on the order of 0.5–0.7 eV for 4d and 0.5 eV for 5d TM ions [1]. Both tendencies work hand in hand in stabilizing orbital-selective states.

6. Spin–orbit-related effects

6.1 Spin–orbit coupling versus Jahn–Teller effect

As already considered in Section 3.5, strong effects due to the SOC are expected for partially filled t_{2g} bands, for which the orbital moment is not quenched. In this case, we generically have a (triple) orbital degeneracy, and the concomitant Jahn–Teller effect — a structural distortion with a decrease in symmetry — should remove this orbital degeneracy. But we saw that the SOC also chose a particular orbital occupation, which can also lift orbital degeneracy. An important question is what the possible interplay is of the JT effect and the SOC in different situations.

6.1.1 Weak SOC and mean field treatment. For systems with large spins, we can get in many cases a reasonable description of the role of the SOC and the interplay between the SOC and the JT-driven orbital ordering if, instead of formula (19), we treat the SOC classically, or in the mean-field approximation, keeping only the terms of the form $\lambda l^z s^z$. This can be done for several ions from the end of the 3rd row for which we typically have a high-spin state. In such cases, one can face a situation with partially filled t_{2g} bands and simultaneously large total spin. This is, for example, the situation for Co^{2+} ($t_{2g}^5 e_g^2$, $S = 3/2$) or Fe^{2+} ($t_{2g}^4 e_g^2$, $S = 2$) ions. One can easily show that in this case for partially filled t_{2g} levels the SOC and the JT distortions lead to the different splitting of the d-levels and to the opposite distortions of ML_6 octahedra.

Let us consider, for example, the case of one 'extra' t_{2g} electron with the spin 'down' (while there are also 5 electrons in the spin 'up' channel, giving a large total spin) and octahedral geometry, as, e.g., for the high-spin state of Fe^{2+}. The JT effect would remove three-fold orbital degeneracy in such a way that the doubly occupied xy-level goes down (by E_{JT}), and the half-filled doubly degenerate xz- and yz-levels go up (by $E_{JT}/2$). This corresponds to a tetragonal compression of ML_6 octahedra (Fig. 8b). Then, we gain the JT energy $-E_{JT}$. But the occupied xy-orbital here is the orbital with $l^z_{\text{eff}} = 0$, i.e., the SOC coupling $\lambda l^z s^z$ does not give any energy gain under these conditions.

If instead of local compression we have local elongation of the ML_6 octahedron, the level structure will be completely different (see Fig. 8a). Doubly degenerate xz- and yz-levels, or their complex linear combinations $|l^z = \pm 1\rangle = (1/\sqrt{2})(xz \pm \mathrm{i}yz)$, go down by the energy $-E_{JT}/2$. Now, however, the SOC can lead to further splitting of these levels, by the quantity λ, i.e., the ground-state energy gain for the 'extra' electron in this case is $E = -E_{JT}/2 - \lambda/2$. Thus, the deformation in this case would go along the 'JT route' (local contraction, $c/a < 1$) if $E_{JT} > \lambda$, and along the 'SOC route' (local elongation, $c/a > 1$) in the opposite case. We see that in this case the JT effect and the SOC tend to cause opposite types of distortions, and they lead to occupation of different orbitals. It should be recognized that the same situation also exists for other fillings of t_{2g} levels and even in other local surroundings, e.g., in tetrahedra (see book [3]).

Experiments show that for heavier 3d-elements, such as Fe and Co, the larger SOC usually wins and the distortions follow the SOC route. Such is, for example, the situation in FeO and CoO, or in $KFeF_3$ and $KCoF_3$. CoO is especially interesting, since this compound possesses a very large magnetostriction exactly due to this effect. Forming a long-range magnetic order in it below $T_N \sim 300$ K results in cooperative lattice distortions with $c/a < 1$ (in $CO^{2+}(d^7)$ there is an extra hole rather than an extra electron in the t_{2g} shell). Due to a strong interplay with the lattice, the transition itself even becomes a weak first-order transition with a small thermal hysteresis at $T = T_N$ [134].

Note that above we only considered tetragonal distortions. The t_{2g} levels, however, can also be split by trigonal distortions. Experimentally, most Co^{2+}-based compounds are distorted tetragonally, and those of Fe^{2+} do so trigonally. Why this so is not actually clear.

In typical 4d and 5d systems with their low-spin states for TM ions, as well as for 3d systems with a small number of d-electrons, where these electrons reside only at the t_{2g} levels, the situation is different. In this case, we should not consider only terms like $\lambda l^z s^z$, but have to take into account the SOC 'in full force' (with terms like $l^+ s^-$ and $l^- s^+$), also including quantum effects [see Eqn (19)]. The eventual interplay of the JT effect and the SOC then looks different, and the results actually strongly depend on a particular situation, i.e., on the orbital occupation. For the general case, where the strength of the JT coupling (E_{JT}) and the SOC constant λ are comparable, a special detailed treatment has to be carried out. But in the limit of a strong SOC, one can get some results rather easily qualitatively.

6.1.2 Strong SOC: d^4 and d^5 configurations. The first case to consider is the situation already discussed in Section 3.5 for the low-spin d^5 configuration, like that in Ir^{4+}. In the absence of the SOC, this would correspond to one hole in triply degenerate t_{2g} band, and the usual JT effect would lead, e.g., to tetragonal elongation (the level structure is shown in Fig. 8a), with this hole in the xy-orbital (or there can be trigonal distortions, with a hole residing in the a_{1g} orbital). However, in the case of a very strong SOC (jj-coupling), the splitting will be very different: the ground state of such an ion is a Kramers doublet $J = 1/2$, with the wave functions (see Fig. 9)

$$|J_{1/2}, J^z_{1/2}\rangle = \frac{1}{\sqrt{3}}\left(|xy\uparrow\rangle + |(\mathrm{i}xz + yz)\downarrow\rangle\right),$$
$$|J_{1/2}, J^z_{-1/2}\rangle = -\frac{1}{\sqrt{3}}\left(|xy\downarrow\rangle + |(\mathrm{i}xz - yz)\uparrow\rangle\right). \quad (30)$$

Kramers doublets have no extra (orbital) degeneracy, i.e., there would be no JT effect in such a state. Thus, we see that in this case the strong SOC completely suppresses the JT distortions (and vice versa, if we made such distortions, e.g., elongation of the ML_6 octahedron, then a hole would occupy the xy-orbital, which is the state with $l^z_{\text{eff}} = 0$, i.e., such distortion would quench the SOC). It is interesting that while there is no orbital degeneracy in the ground state in the case of a large SOC for the d^5 configuration, it still exists in the excited states [135].

The situation for the t_{2g}^4 configuration in the case of a strong SOC is very similar. Without the SOC, we would again

have orbital degeneracy, and corresponding JT distortion would be a tetragonal compression of ML_6 octahedra (or similar trigonal distortion), for which the xy-singlet (or a_{1g} for trigonal distortion) would go down and would be filled by two electrons, while the xz, yz doublet (or e_g^{π} doublet) lying above would have two electrons with parallel spins (see Fig. 8b). But the SOC would prefer a very different orbital filling — the one shown in Fig. 9, with the singlet ground state $J = 0$. Thus, in this case, the strong SOC will also suppress the JT effect.

6.1.3 Strong SOC: d^1 and d^2 configurations. However, the situation becomes much different for d^1 and d^2 configurations. In this case, for a less-than-half-filled t_{2g} subshell, the third Hund's rule tells us that the order of multiplets is inverted, and the lowest-energy state would be a quartet $J = 3/2$ (the same conclusion is also valid in the *jj*-coupling scheme (see Section 3.5)). The one-electron states of the $J = 3/2$ quartet are two Kramers doublets:

$$|J_{3/2}, J^z_{3/2}\rangle = |l^z = 1, \uparrow\rangle = -\frac{1}{\sqrt{2}}\left(|yz, \uparrow\rangle + \mathrm{i}|xz, \uparrow\rangle\right),$$

$$|J_{3/2}, J^z_{-3/2}\rangle = |l^z = -1, \downarrow\rangle = \frac{1}{\sqrt{2}}\left(|yz, \downarrow\rangle - \mathrm{i}|xz, \downarrow\rangle\right),$$

$$|J_{3/2}, J^z_{1/2}\rangle = \sqrt{\frac{2}{3}}\,|l^z = 0, \uparrow\rangle - \frac{1}{\sqrt{3}}\,|l^z = 1, \downarrow\rangle$$

$$= \sqrt{\frac{2}{3}}|xy, \uparrow\rangle - \frac{1}{\sqrt{3}}\left|\frac{1}{\sqrt{2}}(yz + ixz), \downarrow\right\rangle,$$

$$|J_{3/2}, J^z_{-1/2}\rangle = \sqrt{\frac{2}{3}}\,|l^z = 0, \downarrow\rangle + \frac{1}{\sqrt{3}}\,|l^z = -1, \uparrow\rangle$$

$$= \sqrt{\frac{2}{3}}|xy, \downarrow\rangle + \frac{1}{\sqrt{3}}\left|\frac{1}{\sqrt{2}}(yz - ixz), \uparrow\right\rangle. \quad (31)$$

In effect, there is not only a Kramers degeneracy, but also an extra (orbital) degeneracy (notice that it is not a triple degeneracy as in the original t_{2g} shell, but a double degeneracy — two Kramers doublets!). This extra degeneracy can again be removed by distortions caused by the same JT effect.

Without the SOC, of course, these configurations, d^1 and d^2, are JT-active, leading to opposite distortions (tetragonal compression for d^1, and tetragonal elongation for d^2). Interestingly enough, one can show that in the case of a strong SOC, when $\lambda \to \infty$, the still present JT distortion should be such that both tetragonal elongation and compression of ML_6 octahedra give the same energy of the distorted state in the first approximation (this reminds the formation of the 'Mexican hat' in the JT effect for doubly degenerate e_g; for the triply degenerate t_{2g}, the situation is very different). The large but finite λ would lead to the lowering of the energy of the tetragonally compressed structure for the d^1 configuration, and to elongation at the d^2 configuration — the same as for a pure JT effect at $\lambda = 0$. However, nonlinear effects, such as local anharmonism [136], could change the situation.

Thus, we see that in this case even a very strong SOC does not completely suppresses JT distortion, but still reduces it: due to the presence of Clebsch–Gordan coefficients $\sqrt{2/3}$, etc. in expressions (31) describing wave functions for the $J = 3/2$ quartet, the JT energy gain turns out to be half of what one would get without the SOC.

6.1.4 Strong SOC: d^3 configuration. A very unusual situation takes place for the d^3 configuration, for a nominally half-filled t_{2g} shell. In the ordinary *LS* coupling scheme, we would then have the $S = 3/2$ state with a quenched orbital momentum $L = 0$ and without the SOC (in the first approximation). However, the situation would be very different for a strong SOC, in the *jj*-coupling scheme. It has been mentioned in Section 3.5 that for the d^3 configuration these two coupling schemes, *LS* and *jj*, lead in general to different states: the pure spin $S = 3/2$, $L = 0$ quartet in the *LS* coupling scheme, and the spin–orbit-determined $J = 3/2$ quartet in the *jj*-scheme, with different wave functions and, generally speaking, with different physical parameters, such as the *g*-factors. Furthermore, from the point of view of the JT effect, these two states are different. There is no orbital degeneracy left for the half-filled t_{2g} shell in the *LS* coupling scheme. However, this is not the case in the *jj*-scheme. Again, we have here *two* Kramers doublets $|J_{3/2}, J^z_{\pm 3/2}\rangle$ and $|J^z_{3/2}, J^z_{\pm 1/2}\rangle$, with different wave functions [see formula (31)], and with different (opposite) local JT distortions. If we put three electrons in these states, one of these doublets would be necessarily filled, but another half-filled, so that the total distortions would not cancel, and such a d^3 configuration would again be JT-active and would lead to the JT distortion!

We see that in this case, in contrast to the situation in Section 6.1.2, the SOC does not suppress, but activates (causes) JT distortion! It would be very interesting to confirm these considerations experimentally. The absence/presence of the JT effect for the d^3 configuration could be a fingerprint of the applicability of the *LS* (Russel–Saunders) or *jj*-coupling schemes for a particular material.

6.2 Spin–orbit coupling and the formation of 'molecules' in solids

Similarly to the JT effect discussed in the previous section, the SOC can influence the formation of MO states in solids, discussed in Sections 4.3 and 5.2. Again, the detailed results depend on the particular situation. Generally, one should expect that a strong SOC would act against the formation of bonding states, for example, in TM dimers. But here there are exceptions.

Consider, for example, the case of the common edge geometry shown in Fig. 6b, for which only the xy-orbitals can form the bonding MO state (we ignore here possible hoppings between the xz- and yz-orbitals via oxygen). We gain maximum bonding energy when electrons occupy these xy-orbitals. But the SOC may favor very different orbitals. For example, in the case of a d^1 configuration, strong SOC would stabilize an electron in a $J = 3/2$ quartet [Eqn (31)]. In this case, the Kramers doublet $|J_{3/2}, J^z_{\pm 3/2}\rangle$ does not form bonding states at all (xy-orbitals do not enter the states of this doublet). Only the doublet $|J_{3/2}, J^z_{\pm 1/2}\rangle$, containing the xy component, would contribute to the bonding. Both these xy-orbitals enter the $|J_{3/2}, J^z_{\pm 1/2}\rangle$ wave function with the coefficient $\sqrt{2/3}$ [see (31)]. Correspondingly, the bonding energy in this case would be reduced; it would be $-2/3t$ instead of $-t$ for the real xy-orbital. Thus, we see that in this case the strong SOC leading to the formation of the $J = 3/2$ quartet partially suppresses the tendency towards MO formation.

The same arguments would work not only for a single electron, but also for a single hole in the t_{2g} shell, such as Ir^{4+} ions. According to Eqn (30), the 'active' xy-orbital only enters in this case the $J = 1/2$ wave function with an even smaller coefficient, $1/\sqrt{3}$, so that, in effect, the bonding energy would be reduced even more significantly, by a factor of 3: $E_{\mathrm{bond}} = -t/3$.

For other electronic configurations, such as d^2 or d^3, the situation could be even trickier. One also then has to worry about the role of the Hund's coupling. We have seen in Section 5.2 that the Hund's coupling counteracts the kinetic energy (hopping), i.e., it acts against MO formation. But in general, it may also work against the SOC, since the Hund's exchange maximizes the spin S, while the SOC takes care of the total momentum J. We will not discuss these different cases here; it suffices to say that the features of MO formation in correlated materials, especially for those of 4d and 5d elements, can also be sensitive to the SOC; and vice versa, strong intersite effects could, in principle, suppress the SOC.

6.3 $J_{\rm eff} = 1/2$ and the spin–orbit-assisted Mott state

Usually, when we go down a column in the Periodic Table, e.g., from Co to Rh and to Ir, a larger spatial extension of the 4d and 5d orbitals (compared with 3d) and stronger covalency lead to a more pronounced metallic behavior. However, in Sr_2MO_4 systems, the tendency is the other way around. While Sr_2CoO_4 (quite difficult to prepare) and Sr_2RhO_4 are metallic [137, 138], Sr_2IrO_4 is insulating [139]. It turns out that one needs to take into account the SOC when describing this behavior.

The electronic configuration of these TM ions is d^5. Due to a large $t_{2g} - e_g$ crystal-field splitting, all these electrons occupy t_{2g} levels. As has been shown in Section 3.5, a strong SOC removes orbital degeneracy, and the ground state will be the Kramers doublet $J_{\rm eff} = 1/2$. The situation will then become essentially equivalent to that of a half-filled non-degenerate Hubbard model, described by Eqn (3) [140]. The critical U_c for the Mott transition for these $J_{\rm eff} = 1/2$ states is smaller than that for the whole d-band, since, first of all, $U_c \sim \sqrt{N}U_{c,0}$ [141], where N is the orbital degeneracy ($N_{J_{\rm eff}} = 1$, while $N_{t_{2g}} = 3$). Second, the width of the $J_{\rm eff} = 1/2$ band is smaller than the width of the whole t_{2g} band [140]. This explains why Sr_2IrO_4 is a (Mott) insulator, whereas Sr_2CoO_4 and Sr_2RhO_4 are metallic [140]. The last cited paper started the whole activity in studying correlated solids with strong SOC, which has led to some quite interesting and nontrivial results.

6.4 Spin–orbit-driven Peierls transition

After the discovery of the strong influence of the SOC on the Mott transition, it became clear that the SOC can also be very important for many other physical effects, e.g., for the Peierls effect. Indeed, these are the Peierls distortions which allowed explaining the highly unusual and seemingly self-contradictory properties of CsW_2O_6. In this compound, W ion valency is 5.5+ and nominally one has 1/2 electron per site. In spite of noninteger occupancy, it is a nonmagnetic insulator in the low-temperature phase (below 210 K) [142]. Because of the large t_{2g} bandwidth, this fact cannot be explained by Hubbard correlations [142]. The solution to this problem came with the account of SOC coupling, which greatly modifies the band structure, making it susceptible to the Peierls transition [143]. The Fermi surface exhibits strong nesting, in this case, while the electronic (Lindhard's) susceptibility shows clear divergence at the same $\mathbf{q}$ vector. Calculations of the phonon spectra and the subsequent lattice optimization allowed us to find the crystal structure with tetramerized W–W chains running in two orthogonal directions in two different *ac* planes. CsW_2O_6 turned out to be a nonmagnetic band insulator in this picture, which fully explains all experimental findings.

While it is hard to single out any 1D bands in CsW_2O_6, even taking into account the SOC, one might propose a very simple model which explains the Peierls instability in this compound and the importance of the SOC. The β-pyrochlore structure of CsW_2O_6 resembles a spinel (with TM ions at the B-sites), which are prone to the Peierls distortions due to '1D-zation' of the electronic spectrum, as we have seen in Section 4.2. Here, WO_6 octahedra are elongated and thus electrons occupy two degenerate xz/yz bands. The SOC removes this degeneracy, and we have 1/2 electron in the doubly degenerate (taking into account spin) band, which naturally explains the tetramerization found in the band structure calculations.

6.5 Kitaev exchange

One of the most interesting consequences of strong SOCs is the conclusion reached by Jackeli and Khaliullin [144] that d^5 systems with a honeycomb lattice such as Li_2IrO_3, Na_2IrO_3 or α-$RuCl_3$ might exhibit a very unusual type of exchange interaction, which is nowadays called the Kitaev interaction. Instead of using the Heisenberg model (4), it can be described by the Hamiltonian

$$H = \sum_{ij} K_{ij} S_i^{\gamma} S_j^{\gamma} . \tag{32}$$

For each bond, this interaction is of an Ising character, but with different S components (numbered by the subscript $\gamma = \{x, y, z\}$) 'working' on different bonds (Fig. 27). Such a model, called there the 'compass model', was first introduced in review [7] in treating orbital ordering, and anisotropic exchange there was caused by the directional character of orbitals, mentioned many times above in this review. Kitaev independently formulated this model in paper [145], and, most importantly, showed that on a honeycomb lattice this model can be solved exactly, and the solution displays quite nontrivial states, such as the spin-liquid state with short-range correlations, Majorana fermion, etc. These results attracted enormous attention (see, e.g., Ref. [146]), especially because one could think of using the special properties of such systems for quantum computations [145, 147]. It was shown in Ref. [144] that honeycomb materials with a t_{2g}^5 electronic configuration (Ir^{4+} or Ru^{3+} ions) could be real examples of Kitaev systems.

The origin of the bond-dependent interaction (32) is explained in Fig. 28. It may be seen that a single hole resides on $J = 1/2$ levels in the case of a strong SOC (Fig. 9). As follows from Fig. 28, there are two equivalent paths for virtual hopping (via p_z orbitals of ligands) from one Ir to

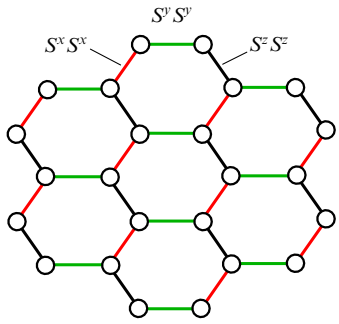

Figure 27. Kitaev model on a honeycomb lattice.

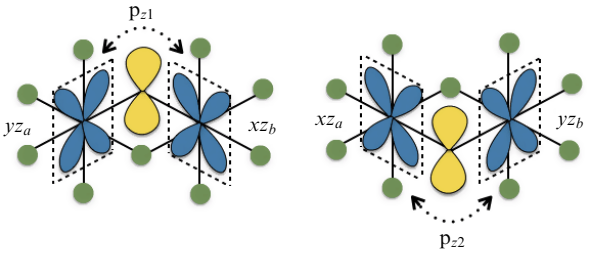

Figure 28. Possible exchanges paths between two t_{2g} orbitals via the ligand p_z-orbital in the common-edge geometry.

another in the edge-sharing geometry, which usually leads to an (antiferromagnetic) superexchange. However, for a strong SOC, with wave functions (30), the total effective hopping between these wave functions (30), t_{dd}^{eff}, exactly cancels due to the presence of i for one of the relevant d-orbitals. This is why conventional superexchange given by formula (15) does not work in this situation. If one assumes that the direct exchange between t_{2g} orbitals is zero, then what remains is the higher-order processes (hopping to empty orbitals, with the Hund's rule acting there). These higher-order processes lead to the Ising-like interaction $KS_i^z S_j^z$ for the xy-plaquettes of Fig. 28, and to similar interactions with KS^xS^x for the yz-plaquettes (bonds) and KS^yS^y for the zx bonds, where S is the effective spin $S = 1/2$ for a $J = 1/2$ Kramers doublet [144]. The exchange constant is given by

$$K \sim \frac{t_{pd}^4}{\Delta_{CT}^2 U}\frac{J_H}{U}\,, \tag{33}$$

very similar to what we obtained in formula (16).

For real honeycomb materials like Na_2IrO_3 or α-$RuCl_3$, different Ir–Ir or Ru–Ru bonds have different orientations (see Fig. 28), so that, in effect, on three bonds going from each Ir or Ru ion we get S^zS^z interactions for one bond, S^xS^x for another, S^yS^y for the third, i.e., the Kitaev model (32).

Deviations from the exact cubic symmetry or from 90° metal–ligand–metal angle, as well as some other exchange processes, e.g., due to direct d–d hopping of the xy-orbitals, would also add to this interaction some Heisenberg terms, so that the resulting model becomes Heisenberg–Kitaev. Also, the exchange processes important for charge-transfer insulators [see formula (14) and Fig. 4b (with virtual states with two holes on one oxygen)] would give Heisenberg terms in the exchange (each exchange pass, via each oxygen, acts here independently, so that there would be no interference terms and no cancellation of hoppings leading to the Heisenberg interaction; see also Ref. [144]).

The question of the relative importance of Heisenberg or Kitaev terms, as well as the possible role (and the form) of more distant interactions for different real materials, is a matter of active experimental and theoretical study (see, e.g., review [147]).

6.6 Singlet (or excitonic) magnetism

The situation with ions possessing the d^4 configuration for 4d and 5d materials with a strong SOC deserves special consideration. Ir^{5+} and Ru^{4+}, for example, are such ions. According to the treatment presented above, such isolated ions in a cubic crystal field should have a nonmagnetic singlet ground state with $J = 0$. And, indeed, Ir^{5+} is a famous nonmagnetic ion: for ESR (electron spin-resonance) people it is a classical ion for nonmagnetic dilution. However, it is, in principle, still possible that a magnetic state of such ions and even long-range magnetic ordering may exist; for example, it is typical for insulating Ru^{4+} compounds, e.g., Ca_2RuO_4 and Na_2RuO_3 are antiferromagnets at low temperatures [148, 149]. This may be a typical case of a singlet magnetism (see, e.g., Section 5.5 in monograph [1]).

Indeed, first of all, the SOC may be partially quenched by lattice distortions, which lead to a noncubic crystal field. Then, the exchange interaction with neighboring ions could be strong enough, so as to overcome the initial splitting of the ground-state nonmagnetic singlet $J = 0$ and the excited triplet $J = 1$: if Zeeman splitting of such a triplet (by the internal exchange field from all other ions) exceeds the splitting between the $J = 1$ and $J = 0$ states (given by λ), a magnetic state would have lower energy. This is the typical situation of singlet magnetism, well known for many rare-earth compounds, e.g., those with Pr.

Recently, this topic became popular after a suggestion by G Khaliullin [150] that many d^4 systems, for example, those with Ru^{4+}, can be described by this model; he called the resulting magnetic state an excitonic magnet.

The phenomenological description of the resulting magnetic state of materials like Ca_2RuO_4 is still possible with the usual exchange Hamiltonian for $S = 1$, but containing strong anisotropic terms [151–153]. Additionally, there are also interesting new predictions, such as the existence of a new spin-wave mode for 'soft' spins, which may be called the Higgs mode. It seems to be observed in Ca_2RuO_4 in paper [153].

7. Conclusions

The interplay between the spin, charge, and lattice degrees of freedom in transition metal compounds gives rise to various important physical effects, such as giant magnetoresistance, high-temperature superconductivity, and many others. An account of the directional character of orbitals additionally enriches physical phenomena met in these systems. It turns out that in many cases orbitals play the role of either a transmitter, which establishes a link among magnetic, electronic, and elastic properties, or a tuner, which regulates interplay among them.

As an example of the first role, one may recall the Jahn–Teller effect, which couples electronic and elastic properties, or the presence of magnetic anisotropy, which is usually related to the spin–orbit interaction. The second role of orbitals as a fine tuner has become more and more important in recent years. Thus, as we have seen, these are orbital degrees of freedom that tune the exchange interaction in honeycomb systems like Na_2IrO_3 or α-$RuCl_3$ and may result in Kitaev physics with a spin-liquid ground state and highly unusual excitation spectra. It is indeed rather interesting that Kitaev first solved his exotic model and found some nontrivial implications, and only later was it realized that the orbital degrees of freedom can tune a system to the regime where it can be described by this model. We expect that this second role of orbitals will become increasingly important, both since it opens new perspectives for fundamental science and due to possible technological applications. In particular, one might think of 'orbital engineering' on surfaces, interfaces, etc.

Another tendency in orbital physics, which has to be mentioned, is the change in the general route. Previously,

most of the activity in this field was concentrated on the study of spin-orbital entanglement in Kugel–Khomskii-like Hamiltonians due to superexchange or on the analysis of the magnetic properties of different materials due to the celebrated Goodenough–Kanamori–Anderson rule, or was connected with the interplay between orbital and lattice degrees of freedom via the Jahn–Teller effect. In recent years, however, a very different class of phenomena has come to the forefront, first of all, specific phenomena due to the directional character of orbitals. Second, this is the influence of orbital degrees of freedom on 'classical' effects, e.g., Mott and Peierls transitions. Third, a lot of studies are now concentrated on phenomena related to the spin–orbit coupling. We have found that the spin–orbit coupling can be important for almost all the effects we know in condensed matter physics: superconductivity, the Jahn–Teller and Peierls effects, and the Mott transition; it also results in spin–orbit entanglement as in the case of the superexchange interaction and leads to pronounced exchange anisotropy. One may expect that the list of these phenomena will only widen in the coming years.

In this review, we tried to describe a novel development in the field of orbital physics. We hope that we demonstrated that this part of condensed matter physics, though not new, is still a very active field of research and is able to produce new surprises.

This work was supported by the Russian Science Foundation through project 17-12-01207.

* * *

Only a year ago, we published a paper in the special issue of *JETP* devoted to the 85th birthday of Leonid Veniaminovich Keldysh. Unfortunately, now we have to write a paper for the memorial issue of *UFN*. One of us, D Kh, was one of his first PhD students, and later for many years he was a member of his sector at the Department of Theoretical Physics at the Lebedev Physical Institute of the Academy of Sciences. The interaction with L V Keldysh over many years was really crucial for his development. Both of us express deep sorrow at the loss of L V, and we are sure that the memory of L V Keldysh, both as a brilliant physicist and a wonderful person, will remain with us for many years to come.

References

1. Khomskii D I *Transition Metal Compounds* (Cambridge: Cambridge Univ. Press, 2014)
2. Imada M, Fujimori A, Tokura Y *Rev. Mod. Phys.* **70** 1039 (1998)
3. Goodenough J B *Magnetism and the Chemical Bond* (New York: Interscience Publ., 1963)
4. Fazekas P *Lecture Notes on Electron Correlation and Magnetism* (Ser. in Modern Condensed Matter Physics, Vol. 5) (Singapore: World Scientific, 1999)
5. Khomskii D I *Basic Aspects of the Quantum Theory of Solids*: *Order and Elementary Excitations* (Cambridge: Cambridge Univ. Press, 2010)
6. Khomskii D I *Fiz. Met. Metalloved.* **29** 31 (1970)
7. Kugel' K I, Khomskii D I *Sov. Phys. Usp.* **25** 231 (1982); *Usp. Fiz. Nauk* **136** 621 (1982)
8. Zaitsev R O, Kuz'min E V, Ovchinnikov S G *Sov. Phys. Usp.* **29** 322 (1986); *Usp. Fiz. Nauk* **148** 603 (1986)
9. Izyumov Yu A *Phys. Usp.* **38** 385 (1995); *Usp. Fiz. Nauk* **165** 403 (1995)
10. Nussinov Z, van den Brink J *Rev. Mod. Phys.* **87** 1 (2015)
11. Oleś A M *J. Phys. Condens. Matter* **24** 313201 (2012)
12. Bulaevskii L N *Sov. Phys. Usp.* **18** 131 (1975); *Usp. Fiz. Nauk* **115** 263 (1975)
13. Mott N F, Peierls R *Proc. Phys. Soc.* **49** 72 (1937)
14. Coulson C A, Fischer I *Philos. Mag.* **40** 386 (1949)
15. Ushakov A V, Streltsov S V, Khomskii D I *J. Phys. Condens. Matter* **23** 445601 (2011)
16. Korotin M A, Anisimov V I, Khomskii D I, Sawatzky G A *Phys. Rev. Lett.* **80** 4305 (1998)
17. Señarís-Rodríguez M A, Goodenough J B *J. Solid State Chem.* **116** 224 (1995)
18. Korotin M A et al. *Phys. Rev. B* **54** 5309 (1996)
19. Haverkort M W et al. *Phys. Rev. Lett.* **97** 176405 (2006)
20. Kuneš J, Křápek V *Phys. Rev. Lett.* **106** 256401 (2011)
21. Streltsov S V, Khomskii D I *Phys. Rev. B* **86** 064429 (2012)
22. Khalifah P et al. *Science* **297** 2237 (2002)
23. Wu H et al. *Phys. Rev. Lett.* **96** 256402 (2006)
24. Zhou H D et al. *Phys. Rev. B* **85** 041201(R) (2012)
25. Streltsov S V *Phys. Rev. B* **88** 024429 (2013)
26. Hester J R et al. *Acta Cryst. B* **53** 739 (1997)
27. Cwik M et al. *Phys. Rev. B* **68** 060401(R) (2003)
28. Streltsov S V et al. *Phys. Rev. B* **71** 245114 (2005)
29. Vasiliev A N et al. *Phys. Rev. B* **72** 012412 (2005)
30. Erickson A S et al. *Phys. Rev. Lett.* **99** 016404 (2007)
31. Kanamori J *Prog. Theor. Phys.* **30** 275 (1963)
32. Sugano S, Tanabe Y, Kamimura H *Multiplets of Transition-Metal Ions in Crystals* (New York: Academic Press, 1970)
33. Andersen O K, Klose W, Nohl H *Phys. Rev. B* **17** 1209 (1978)
34. Harrison W A *Elementary Electronic Structure* (Singapore: World Scientific, 1999)
35. Streltsov S V, Khomskii D I *Phys. Rev. B* **77** 064405 (2008)
36. Kugel K I, Khomskii D I, Sboychakov A O, Streltsov S V *Phys. Rev. B* **91** 155125 (2015)
37. Khomskii D I, Kugel K I, Sboychakov A O, Streltsov S V *JETP* **122** 484 (2016); *Zh. Eksp. Teor. Fiz.* **149** 562 (2016)
38. Daoud-Aladine A et al. *Phys. Rev. B* **80** 220402(R) (2009)
39. Reynaud M et al. *Inorg. Chem.* **52** 10456 (2013)
40. Markina M M et al. *Phys. Rev. B* **89** 104409 (2014)
41. Tokura Y, Tomioka Y *J. Magn. Magn. Mater.* **200** 1 (1999)
42. Izyumov Yu A, Skryabin Yu N *Phys. Usp.* **44** 109 (2001); *Usp. Fiz. Nauk* **171** 121 (2001)
43. Zener C *Phys. Rev.* **82** 403 (1951)
44. Anderson P W, Hasegawa H *Phys. Rev.* **100** 675 (1955)
45. Yosida K *Phys. Rev.* **106** 893 (1957)
46. de Gennes P-G *Phys. Rev.* **118** 141 (1960)
47. Kubo K, Ohata N *J. Phys. Soc. Jpn.* **33** 21 (1972)
48. Nagaev E L *JETP* **30** 693 (1970); *Zh. Eksp. Teor. Fiz.* **57** 1274 (1970)
49. Kagan M Yu, Khomskii D I, Mostovoy M V *Eur. Phys. J. B* **12** 217 (1999)
50. Dagotto E *Nanoscale Phase Separation and Colossal Magnetoresistance*: *The Physics of Manganites and Related Compounds* (Springer Series in Solid-State Sciences, Vol. 136) (New York: Springer, 2003)
51. Nishimoto S, Ohta Y *Phys. Rev. Lett.* **109** 076401 (2012)
52. Streltsov S V, Khomskii D I *Proc. Natl. Acad. Sci. USA* **113** 10491 (2016)
53. Longuet-Higgins H C et al. *Proc. R. Soc. London A* **244** 1 (1958)
54. Liechtenstein A I, Anisimov V I, Zaanen J *Phys. Rev. B* **52** R5467 (1995)
55. Streltsov S V, Khomskii D I *Phys. Rev. B* **86** 035109 (2012)
56. Streltsov S V, Khomskii D I *Phys. Rev. B* **89** 201115(R) (2014)
57. Pavarini E, Koch E, Lichtenstein A *Phys. Rev. Lett.* **101** 266405 (2008)
58. Leonov I et al. *Phys. Rev. Lett.* **101** 096405 (2008)
59. Pavarini E, Koch E *Phys. Rev. Lett.* **104** 086402 (2010)
60. Abragam A, Bleaney B *Electron Paramagnetic Resonance of Transition Ions* (Oxford: Clarendon Press, 1970); Translated into Russian: *Elektronnyi Paramagnitnyi Rezonans Perekhodnykh Ionov* (Moscow: Mir, 1972, 1973)
61. Landau L D, Lifshitz E M *Quantum Mechanics. Non-Relativistic Theory* (Oxford: Pergamon Press, 1965) ; Translated from Russian: *Kvantovaya Mekhanika. Nerelyativistskaya Teoriya* (Moscow: Fizmatlit, 2004)
62. Matsuura H, Miyake K *J. Phys. Soc. Jpn.* **82** 073703 (2013)
63. Taylor A E et at. *Phys. Rev. Lett.* **118** 207202 (2017)

64. Kohn W *Rev. Mod. Phys.* **71** 1253 (1999); *Usp. Fiz. Nauk* **172** 336 (2002)
65. Friedel J, in *The Physics of Metals* Vol. 1 *Electrons* (Ed. J M Ziman) (Cambridge: Cambridge Univ. Press, 1969) p. 340
66. van Wezel J, van den Brink J *Europhys. Lett.* **75** 957 (2006)
67. Seidel A et al. *Phys. Rev. B* **67** 020405(R) (2003)
68. Kobayashi K, Kosuge K, Kachi S *Mater. Res. Bull.* **4** 95 (1969)
69. Katayama N et al. *Phys. Rev. Lett.* **103** 146405 (2009)
70. Horibe Y et al. *Phys. Rev. Lett.* **96** 086406 (2006)
71. Uehara A, Shinaoka H, Motome Y *Phys. Rev. B* **92** 195150 (2015)
72. Radaelli P G et al. *Nature* **416** 155 (2002)
73. Khomskii D I, Mizokawa T *Phys. Rev. Lett.* **94** 156402 (2005)
74. Schmidt M et al. *Phys. Rev. Lett.* **92** 056402 (2004)
75. Kugel K I, Khomskii D I *Sov. Phys. JETP* **37** 725 (1973); *Zh. Eksp. Teor. Fiz.* **64** 1429 (1973)
76. Satija S K et al. *Phys. Rev. B* **21** 2001 (1980)
77. Lee S et al. *Nature Mater.* **5** 471 (2006)
78. Gehring G A, Gehring K A *Rep. Prog. Phys.* **38** 1 (1975)
79. Tokura Y, Nagaosa N *Science* **288** 462 (2000)
80. Haldane F D M *Phys. Rev. Lett.* **50** 1153 (1983)
81. Affleck I *J. Phys. Condens. Matter* **1** 3047 (1989)
82. Reehuis M et al. *Eur. Phys. J. B* **35** 311 (2003)
83. Lee S-H et al. *Phys. Rev. Lett.* **93** 156407 (2004)
84. Tsunetsugu H, Motome Y *Phys. Rev. B* **68** 060405(R) (2003)
85. Tchernyshyov O *Phys. Rev. Lett.* **93** 157206 (2004)
86. Maitra T, Valentí R *Phys. Rev. Lett.* **99** 126401 (2007)
87. Pardo V et al. *Phys. Rev. Lett.* **101** 256403 (2008)
88. Streltsov S V *J. Magn. Magn. Mater.* **383** 27 (2015)
89. Anderson D L *New Theory of the Earth* (Cambridge: Cambridge Univ. Press, 2007)
90. Isobe M et al. *J. Phys. Soc. Jpn.* **71** 1423 (2002)
91. Pen H F et al. *Phys. Rev. Lett.* **78** 1323 (1997)
92. Straumanis M E, James W J, Custead W C *J. Electrochem. Soc.* **107** 502 (1960)
93. Korotin M A et al. *Phys. Rev. Lett.* **83** 1387 (1999)
94. Abd-Elmeguid M M et al. *Phys. Rev. Lett.* **93** 126403 (2004)
95. Harris S *Polyhedron* **8** 2843 (1989)
96. Fabrizio M, Tosatti E *Phys. Rev. B* **55** 13465 (1997)
97. Palstra T T M et al. *Solid State Commun.* **93** 327 (1995)
98. Streltsov S, Mazin I I, Foyevtsova K *Phys. Rev. B* **92** 134408 (2015)
99. Mazin I I et al. *Phys. Rev. Lett.* **109** 197201 (2012)
100. Foyevtsova K et al. *Phys. Rev. B* **88** 035107 (2013)
101. Pchelkina Z V, Streltsov S V, Mazin I I *Phys. Rev. B* **94** 205148 (2016)
102. Hiley C I et al. *Phys. Rev. B* **92** 104413 (2015)
103. Tian W et al. *Phys. Rev. B* **92** 100404(R) (2015)
104. Biffin A et al. *Phys. Rev. B* **90** 205116 (2014)
105. Miura Y et al. *J. Phys. Soc. Jpn.* **76** 033705 (2007)
106. Miura Y et al. *J. Phys. Soc. Jpn.* **78** 094706 (2009)
107. Jackeli G, Khomskii D I *Phys. Rev. Lett.* **100** 147203 (2008)
108. Kimber S A J et al. *Phys. Rev. B* **89** 081408(R) (2014)
109. Arapova I Yu et al. *JETP Lett.* **105** 375 (2017); *Pis'ma Zh. Eksp. Teor. Fiz.* **105** 356 (2017)
110. Park J et al. *Sci. Rep.* **6** 25238 (2016)
111. Sachdev S *Quantum Phase Transitions* (Cambridge: Cambridge Univ. Press, 2011)
112. Tocchio L F et al. *J. Phys. Condens. Matter* **28** 105602 (2016)
113. Anisimov V I et al. *Eur. Phys. J. B* **25** 191 (2002)
114. de' Medici L et al. *Phys. Rev. Lett.* **102** 126401 (2009)
115. Biermann S, de' Medici L, Georges A *Phys. Rev. Lett.* **95** 206401 (2005)
116. Koga A et al. *Phys. Rev. Lett.* **92** 216402 (2004)
117. Li S, Khatami E, Johnston S *Phys. Rev. B* **95** 121112(R) (2017)
118. Efremov D V, Khomskii D I *Phys. Rev. B* **72** 012402 (2005)
119. Castellani C, Natoli C R, Ranninger J *Phys. Rev. B* **18** 4967 (1978)
120. Larson M L, Moore F W *Inorg. Chem.* **3** 285 (1964)
121. Kepert D L, Mandyczewsky R *Inorg. Chem.* **7** 2091 (1968)
122. Korotin D M, Anisimov V I, Streltsov S V *Sci. Rep.* **6** 25831 (2016)
123. Torardi C C et al. *J. Solid State Chem.* **60** 332 (1985)
124. Chi L, Britten J F, Greedan J E *J. Solid State Chem.* **172** 451 (2003)
125. Doi Y et al. *J. Solid State Chem.* **161** 113 (2001)
126. Senn M S et al. *Phys. Rev. B* **87** 134402 (2013)
127. Rijssenbeek J et el. *Phys. Rev. B* **58** 10315 (1998)
128. Doi Y, Matsuhira K, Hinatsu Y *J. Solid State Chem.* **165** 317 (2002)
129. Ziat D et al. *Phys. Rev. B* **95** 184424 (2017)
130. Streltsov S V, Khomskii D I *Phys. Rev. B* **89** 161112(R) (2014)
131. Tran T T et al. *J. Am. Chem. Soc.* **137** 636 (2015)
132. Terzic J et al. *Phys. Rev. B* **91** 235147 (2015)
133. Streltsov S V, Cao G, Khomskii D I *Phys. Rev. B* **96** 014434 (2017)
134. Kanamori J *Prog. Theor. Phys.* **17** 197 (1957)
135. Plotnikova E M et al. *Phys. Rev. Lett.* **116** 106401 (2016)
136. Khomskii D, van den Brink J *Phys. Rev. Lett.* **85** 3329 (2000)
137. Matsuno J et al. *Phys. Rev. Lett.* **93** 167202 (2004)
138. Kim B J et al. *Phys. Rev. Lett.* **97** 106401 (2006)
139. Crawford M K et al. *Phys. Rev. B* **49** 9198 (1994)
140. Kim B J et al. *Phys. Rev. Lett.* **101** 076402 (2008)
141. Gunnarsson O, Koch E, Martin R M *Phys. Rev. B* **54** R11026 (1996)
142. Hirai D et al. *Phys. Rev. Lett.* **110** 166402 (2013)
143. Streltsov S V et al. *Phys. Rev. B* **94** 241101(R) (2016)
144. Jackeli G, Khaliullin G *Phys. Rev. Lett.* **102** 017205 (2009)
145. Kitaev A *Ann. Physics* **321** 2 (2006)
146. Trebst S, in *Lecture Notes of the 48th IFF Spring School ''Topological Matter — Topological Insulators, Skyrmions and Majoranas'', Forschungszentrum Julich, Julich, 2017*
147. Kitaev A Yu *Phys. Usp.* **44** (Suppl.) 131 (2001); *Usp. Fiz. Nauk* **171** (Suppl.) 131 (2001)
148. Braden M et al. *Phys. Rev. B* **58** 847 (1998)
149. Wang J C et al. *Phys. Rev. B* **90** 161110(R) (2014)
150. Khaliullin G *Phys. Rev. Lett.* **111** 197201 (2013)
151. Kunkemöller S et al. *Phys. Rev. Lett.* **115** 247201 (2015)
152. Kunkemöller S et al. *Phys. Rev. B* **95** 214408 (2017)
153. Jain A et al. *Nature Phys.* **13** 633 (2017)